AFRL-AFOSR-UK-TR-2012-0054

Exploring the Fundamental of Fatigue in Composites: Opportunities using X-Ray Computed Tomography Imaging

Serafina Consuelo Garcea
Prof. Dr. S. Mark Spearing
Prof. Dr. Ian Sinclair

University of Southampton
Faculty of Engineering and Environment, Materials Science
University Road
Southampton, United Kingdom SO17 1BJ

EOARD Grant 11-3040

Report Date: October 2012

INTERIM Report for 01 October 2011 to 30 September 2012

Air Force Research Laboratory
Air Force Office of Scientific Research
European Office of Aerospace Research and Development
Unit 4515 Box 14, APO AE 09421

REPORT DOCUMENTATION PAGE

Form Approved
OMB No. 0704-0188

1. REPORT DATE *(DD-MM-YYYY)*	2. REPORT TYPE	3. DATES COVERED *(From - To)*
01 October 2012	Interim Report	1 October 2011 - 30 September 2012

4. TITLE AND SUBTITLE

Exploring the Fundamental of Fatigue in Composites: Opportunities using X-Ray Computed Tomography Imaging

5a. CONTRACT NUMBER
FA8655-11-1-3040

5b. GRANT NUMBER
Grant 11-3040

5c. PROGRAM ELEMENT NUMBER
61102F

6. AUTHOR(S)

Serafina Consuelo Garcea
Prof. Dr. S. Mark Spearing
Prof. Dr. Ian Sinclair

5d. PROJECT NUMBER

5e. TASK NUMBER

5f. WORK UNIT NUMBER

7. PERFORMING ORGANIZATION NAME(S) AND ADDRESS(ES)

University of Southampton
Faculty of Engineering and Environment, Materials Science
University Road
Southampton, United Kingdom SO17 1BJ

8. PERFORMING ORGANIZATION REPORT NUMBER

9. SPONSORING / MONITORING AGENCY NAME(S) AND ADDRESS(ES)

European Office of Aerospace Research and Development
Unit 4515 Box 14
APO, AE 09421

10. SPONSOR/MONITOR'S ACRONYM(S)

AFRL/AFOSR/EOARD

11. SPONSOR/MONITOR'S REPORT NUMBER(S)

AFRL-AFOSR-UK-TR-2012-0054

12. DISTRIBUTION / AVAILABILITY STATEMENT

DISTRIBUTION A. Approved for public release; distribution is unlimited.

13. SUPPLEMENTARY NOTES

14. ABSTRACT

The aim of this work emerges from the need to understand damage mechanisms in composite materials, in terms of onset, growth and propagation, and assess fatigue life behavior, using advanced computed tomography techniques. X-ray computed tomography (XCT) has become extremely useful for material science and structural materials studies, due to its capability to allow 3-D reconstruction of the specimen with high resolution, facilitating accurate microstructural and micromechanical characterization of materials. Since fatigue damage in composite laminates is distinctly three-dimensional in character, XCT appears to be a very promising technique to evaluate the micromechanics of fatigue development. The purpose of this project is to exploit XCT and in situ cyclic loading to assess damage and to establish its links with composite residual strength, and assess damage interaction with matrix toughening particles used in aerospace-grade composites. Experimental data will provide information with which numerical models will be calibrated and validated.

This first annual report of the planned 3-year project provides literature review of micromechanics of fatigue damage in composites, overview of XCT imaging, initial results of tension-tension fatigue tests conducted with laboratory and synchrotron-based CT, and qualitative comparison of micromechanical damage between quasi-static and cyclic loading scenarios. Plans for continued study over the next two years are discussed.

15. SUBJECT TERMS

EOARD, fatigue, composites, micromechanics, crack initiation, x-ray computed tomography, digital volume correlation

16. SECURITY CLASSIFICATION OF:			17. LIMITATION OF ABSTRACT	18. NUMBER OF PAGES	19a. NAME OF RESPONSIBLE PERSON
UU					Randall Pollak, Lt Col, USAF
a. REPORT	b. ABSTRACT	c. THIS PAGE	SAR	85	19b. TELEPHONE NUMBER *(include area code)*
UU	UU	UU			DSN 314-235-6115, +44-1895616115

Standard Form 298 (Rev. 8-98)
Prescribed by ANSI Std. Z39.18

Exploring the Fundamental of Fatigue in Composites: Opportunities using X-Ray Computed Tomography Imaging

Nine Month Report

Supervised by
Prof. Dr. S. Mark Spearing
Prof. Dr. Ian Sinclair

Serafina Consuelo Garcea

Materials Science
Faculty of Engineering and Environment
University of Southampton

September 2012

Table of Contents

Chapter 1 Background

1.1 Introduction

Fibre-reinforced polymer matrix composite materials are employed in aerospace applications [1] and increasingly in other sectors such as sustainable energy (e.g. wind turbines and hydrogen/CNG cylinders), surface transportation (trains, automotive, marine applications), sports equipment and healthcare (diagnostic equipment and orthopaedic devices). They are widely used for primary structures where the specific strength and specific modulus are important, such as aircraft wings. These structures are often subjected to dynamic loadings, which have the potential to cause fatigue degradation of the material. In the past fatigue on composite materials was not considered a problem, because it was believed that the limitations imposed in design for static loads and impact, resulted in service load levels that were not able to generate fatigue failure [2]. At present underpinning mechanics of fatigue are not well known, despite many efforts by researchers.

Fatigue design methodologies are well-established for structures fabricated from essentially homogeneous metallic alloys, whose fatigue failure is typically characterised by growth of a dominant crack, which eventually causes ultimate failure [3]. Therefore, it is considered possible to estimate, for a given set of load conditions, the crack's critical length, intervals of inspections and corresponding proper inspection methods.

Currently this is not possible for composite materials. The principal difficulty is the progression of failure due to multiple interacting damage modes rather than a single identifiable crack. This is further complicated by the inability to inspect for critical damage using purely visual means. As a consequence of these inadequacies, a range of overly-conservative design methods are used in practice [2]. A key to improving this situation is to understand better the fatigue damage processes in composite materials, and their relationship to structural failure.

1.2 Motivation of this work

The aim of this work emerges from the need to understand damage mechanisms in composite materials, in terms of onset, growth and propagation, and assess fatigue life behaviour, using advanced computed tomography techniques.

Various non-destructive techniques are applied to investigate damage in composite laminates, such as ultrasonic testing, thermography, interferometers, and acoustic emission. However, none of these techniques provides micrometre resolution three-dimensional direct observations of damage. X-ray computed tomography (XCT) has become extremely useful for material science and structural materials studies, due to its capability to allow three-dimensional reconstruction of the specimen with high resolution, facilitating microstructural and micromechanical characterization of materials in 3-D. Since fatigue damage in composite laminates is distinctly three-dimensional in character, X-ray computed tomography appears to be a very promising technique to evaluate the micromechanics of fatigue development. The purpose of this project is to exploit X-ray computed tomography and *in situ* cyclic loading to assess damage and to establish its links with composite residual strength. Experimental data will provide information with which numerical models will be calibrated and validated.

Chapter 2 Literature Review

2.1 Fatigue in Aerospace Applications

It was commonly reported in the 1960's and 70's that carbon epoxy reinforced fibre did not suffer from fatigue [2]. As such, aircraft design using composites has generally been based on static properties, impact damage tolerance and compressive behaviour. Fatigue behaviour was not considered an issue, as it was believed that the relevant strain conditions did not produce fatigue damage growth. Today fatigue in composite aircraft structures is recognised as potential problem, if only because airframes are required to last longer in service and it would be preferable to retire structures "for cause" as part of a damage tolerance-based approach to design and operation, rather than based on a pre-determined "safe life". The lack of valid prediction failure methods has generally led to use overestimated safety factors [2]. Davies and Curtis [2] report the approach used in the past to design components subjected to dynamic loads in the aerospace industry, highlighting the main problem connected with this. In particular, they explained that design based on peak tensile strain vs. cycle to failure curves (S-N curves) for unidirectional composite materials, is an inappropriate approach, due to the fact that unidirectional materials exhibit a different behaviour compared to laminates. In fact, for unidirectional materials, loaded in tension, fibres carry almost the entire load and, therefore, fatigue behaviour depends only on the fibre properties. Since carbon fibres are not affected by fatigue loading, consequently composite material should not be sensitive to fatigue. Nevertheless, unidirectional fibre reinforced laminates are used increasingly in aerospace applications, which means that more lamina are layered in a particular stacking sequence with different orientation with the aim to carry the principal stresses. As the fraction of off-axis fibres increases in a laminate, a corresponding reduction of properties arises due to the presence of less fibres that support the applied stress in a given direction. Furthermore, for layers with off-axis fibres, properties are more dependent on the resin response, which results in a more fatigue-sensitive response. For instance, Davies and Curtis [2], reported the S-N curves for unidirectional carbon fibre reinforced by different matrix materials, Figure 2.1, and also how the S-N curves vary with different percentage of unidirectional fibre in a laminate, Figure 2.2.

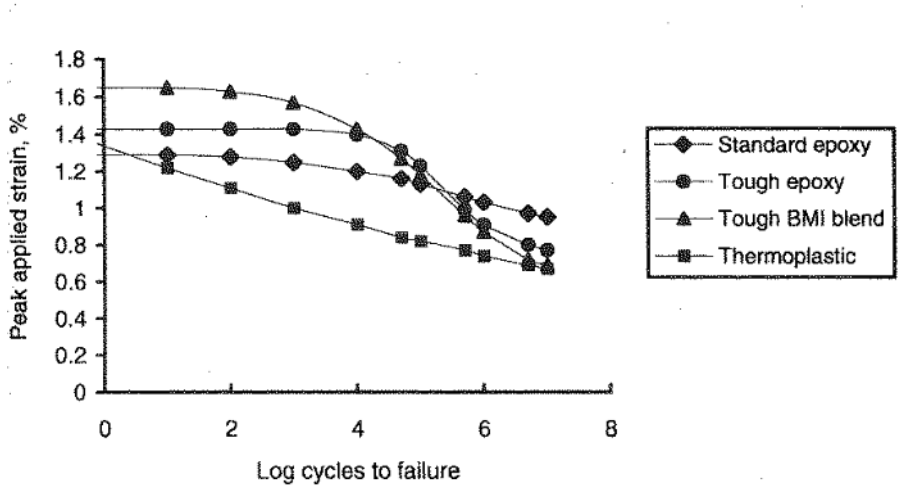

Figure 2. 1 - Typical S-N fatigue curves for unidirectional carbon-fibre composites [2].

Certainly, the percentage of unidirectional plies affects fatigue behaviour; the slope of the S-N curves in Figure 2.2 increases with a decreasing percentage of unidirectional fibre.

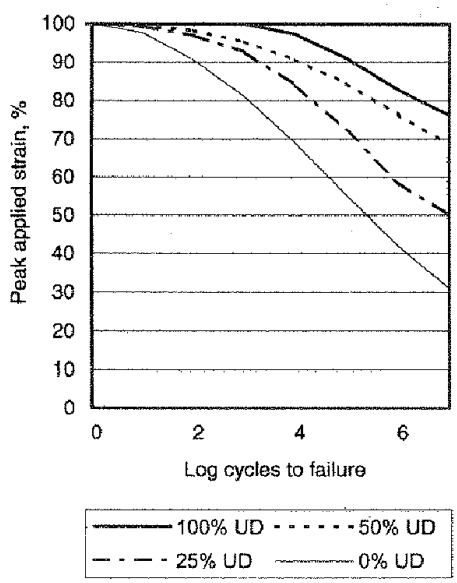

Figure 2. 2 - Effect of the percentage of unidirectional plies on fatigue behaviour [2].

According to S-N curves for unidirectional materials shown in Figure 2.1 after 6-7 million fatigue loading cycles at strains below ~0.6%, fatigue should not be an issue. However, detailed studies have established that this is an incorrect interpretation of fatigue in composites, based on the above-mentioned simplifying assumptions.

A major limiting factor of fatigue in carbon fibre composites for aerospace applications arises under compressive loading [2].

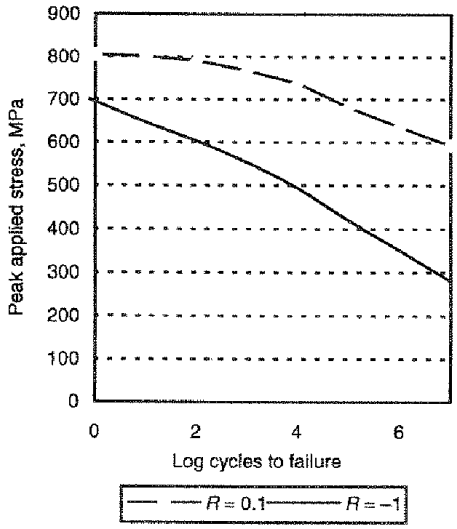

Figure 2. 3 – Comparison between tension-tension and tension-compression loading condition [2].

A critical fatigue loading condition may be identified in symmetric tension-compression (R=-1), which can lead to instability and/or bucking and consequently failure in shorter lifetimes, see Figure 2.3.

2.2 Damage analysis

Fatigue in composites typically involves multiple, spatially distributed, interacting mechanisms, such as transverse ply cracks, splitting in the loading direction, delamination and fibre breaks. Fatigue behaviour is dependent on loading conditions, material, and manufacturing process. Damage mechanisms interact in a frequently non-predictable manner, which is also related to the specific type of laminate. In addition, the intrinsic brittle nature of fibres and variability of manufacturing contribute to the statistical variability in the definition of characteristic parameters. In addition, the critical damage mode or modes, which lead to failure, may be different for each materials configuration and load case.

Micromechanical and macromechanical damage analyses in composite materials have been carried out using several destructive and non-destructive techniques. In this section an overview of damage micromechanisms in composite materials is presented.

2.2.1 Matrix microcracking

The first form of damage often observed in tensile fatigue and static loading of laminates is intralaminar cracking [4, 5, 6], which consists of cracks extending through the thickness of plies, parallel to the fibres within that ply. For the particular case in which cracks are within 90° plies, perpendicular to the loading direction, these microcracks are often referred to as 'transverse ply cracks', or TPCs.

Intralaminar cracks may be observed for static loading, cyclic loading and during changes of temperature [7]. Although, this damage mode is usually not critical in terms of final fracture, it does contribute to reducing the stiffness of the laminate and its strength in the transverse direction, which is particularly significant for components undergoing multi-axial loading [8]. Intralaminar cracking affects the mechanical properties, determining changes in moduli, Poisson ratio, thermal expansion coefficient, and also allows the creation of physical paths by which environmental agents may penetrate bulk material [7]. Furthermore they are indentified to be incipient for other more severe damage modes, such as delamination [4, 5, 7], longitudinal splitting [4, 7] and fibre breakage [5].

Early studies, conducted by Harrison and Bader [4] on carbon fibre reinforced plastics (CFRP) specimens under monotonic and cyclic loading, showed that debonding at the fibre/matrix interface leading to the initiation of transverse ply cracks, as shown schematically in Figure 2.4.

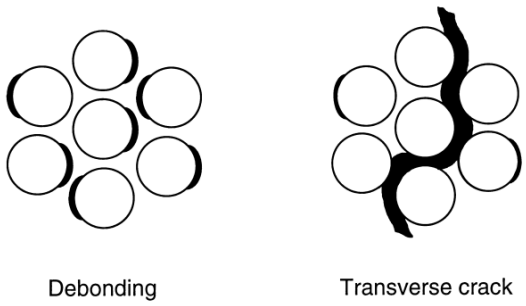

Figure 2. 4 - Schematic representation of debonding and consequently transverse ply crack formation [5].

Dedonding is strictly connected to the adhesion fibre/matrix. In particular, when the matrix shows an elastic-plastic behaviour the generated tensile stress in the matrix is higher than the interfacial shear stress and can induce fibre/matrix debonding [9]. Conversely, when the interfacial bond strength is high, matrix cracking occurs and the composite behaves like a

brittle material [10]. The Poisson effect and the stiffer fibres than the matrix determine an opening zone in compression and a contact zone in tension [5], as represented in Figure 2.4. Further increases in term of stresses cause the coalescence and propagation of debonds, forming transverse ply cracks (Figure 2.5), see [5, 8] also. Vaughan and McCarthy [8] explained coalescence in terms of the creation of small resin bridges between fibres. Increasing load of these bridges causes the resin to undergo plastic deformation until they rupture, causing final failure of the ply. In this context they affirmed that local fibre distribution affected the onset and evolution of debonding. It was demonstrated that debonding phenomena are dependent on the transverse ply thickness. Harrison and Bader [4] found that the formation of cracks appeared to be controlled for thin transverse plies by the fibre/resin debonded, which did not propagate across the section width; while for thicker transverse plies the initiation and propagation of debonding appeared simultaneously.

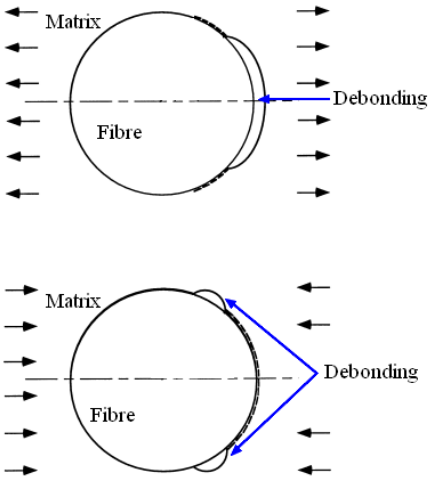

Figure 2. 5 - Debonding for tension and compression case respectively [5].

Previous studies [11, 12] have confirmed that transverse ply cracks are affected by ply thickness, but the authors only described phenomena without giving an explanation of the mechanisms. Garret and Baley [11] performed some experiments on glass fibre matrix reinforced polyester with $[0/90]_s$ layup for different 90° ply thickness. Their results showed the dependence on strain to achieve the first microcrack with 90° ply thickness, as represented in Figure 2.6.

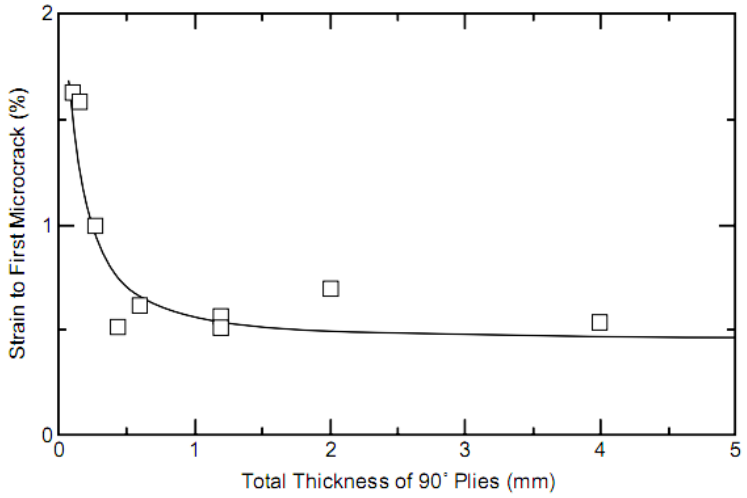

Figure 2. 6 - Strain to achieve the onset microcracking for glass-reinforced [0/90] laminates as a function of the thickness of 90° plies. 0 plies had constant thickness. Data is from Ref. [11].

When 90° ply thickness are greater than 0.5 mm, the initiation and propagation of transverse ply cracks occur simultaneously. For 90° ply thickness thinner than 0.5 mm the strain for initiation increased, in particular between 0.1 mm and 0.4 mm they found single microcracks initiated at the free edge and propagated across the thickness. Finally, for thickness under 0.1 mm no microcracks formation was observed and the laminate failed before transverse microcracks appeared. Similar results were detected for carbon/epoxy laminate by Flaggs and Kural [12] as referenced by [7]. Nairn [7] reported some differences between glass fibre, studied in [11], and carbon fibre, considered in [12], which indicated that in carbon fibre transverse ply cracks appeared instantaneously across the whole section. Regarding the suppression of initiation of transverse ply cracks in matrices reinforced by carbon fibres, they did not report any work in which 90° plies were thinner than half thickness of the 0° plies. This latter thickness was not sufficient to suppress transverse ply cracks.

Many studies [4, 6, 7, 13] reported for both quasi-static and cyclic loading, that transverse ply cracks form by "*edge initiation*", that is cracks initiate at the free edge of the specimens. The reason is the presence of out-of-plane stresses. Nairn *et al*. [14] studied 21 different layups of carbon/epoxy subjected to tensile loading. They considered the damage accumulation in terms of crack density as a function of the loading applied. Results are summarized in Figure 2.7. Symbols represented experimental results, while lines are empirical fits to the experimental data using a fracture mechanics analysis [14].

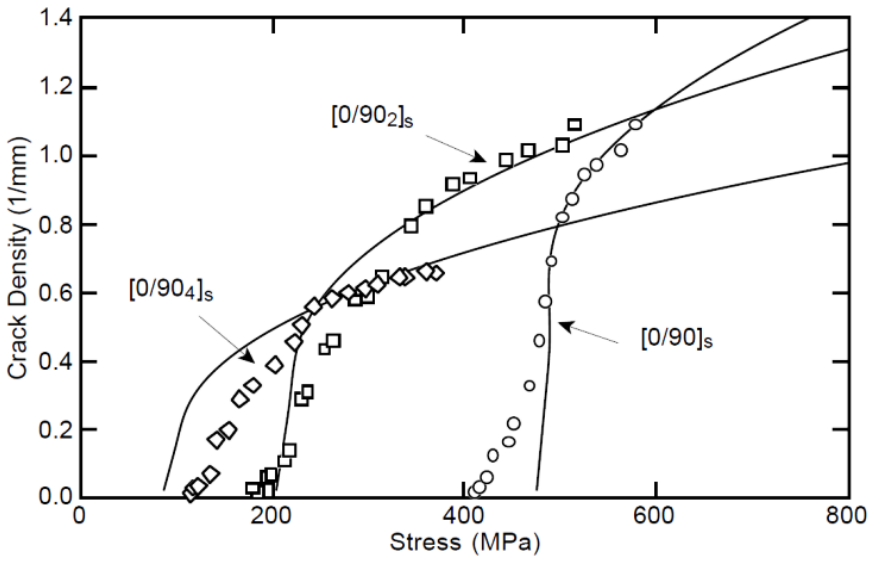

Figure 2. 7 - Microcrack density as a function of the applied stress for carbon/epoxy laminated, characterised by different thickness of the 90° plies. 0° plies thickness was constant. Symbols represent experimental results and lines the data fitting using fracture mechanics methods [14].

Figure 2.7 highlights two important concepts regarding onset and propagation of microcracks for $[0_n/90_m]_s$. First, for each layup configuration no damage detection was reported for a tensile stress lower than a specific threshold, which depended on thickness of 90° plies. In particular, thicker were the 90° plies, and lower was the stress required for microcracks initiation. Specimens had the same thickness for 0° plies. This confirmed the dependence of microcrack initiation on the 90° plies thickness, and also showed that at higher stresses thinner 90° plies developed a greater crack density than thicker 90° plies. Second, considering a specific layup configuration, it is possible to observe the rate of crack propagation. At lower stresses crack density grows rapidly with increasing stress until reaching a near-plateau, at which point further increase in crack density is very limited. This phenomenon was termed "*crack saturation*". They concluded that the saturation crack density was inversely related to the thickness of the 90° plies [7]. Different initial growth rates were verified, and were associated with manufacturing defects and inhomogeneity in the ply material, which varied between specimens [14].

Hobbiebruken *et al.* [15] investigated the influence of adhesion between matrix and fibre on onset and propagation of transverse ply cracks. They considered carbon/epoxy specimens, created by different manufacturing processes and curing temperatures, subjected to three point bending experiments. Results showed that for specimens with high temperature curing, only a small amount of interfacial cracking occurred, after which sudden ply failure in the

transverse direction occurred. Specimens characterised by a low curing temperature exhibited many initial interfacial cracks, linked by small matrix bridges. Further loading produced plastic deformation of matrix bridges, due to shear. Finally, resin bridges break causes failure. Therefore, they indicate that in the case of a weak interface between matrix and fibre, the dominant mechanism was interfacial adhesive failure, while a strong interface determined the mechanism of interphase cohesive failure.

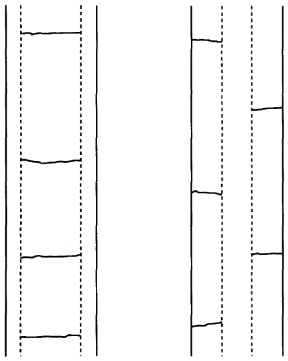

Figure 2. 8 - Transverse ply cracks for $[0/90_4]_s$ and for $[90_4/0_2]_s$ respectively, [14].

Another factor which affects propagation of transverse ply cracks, is known to be staking sequence [4]. Nairn *et al*. [14] showed different damage propagation between configurations that had 90° plies in the middle or on the edge respectively. In particular, when 90° plies were central, cracks developed into one array of periodic microcracks, while when 90° plies were outside, cracks also grouped in periodic microcracks, but arrays were shifted with respect to each other, called "*antisymmetric* or *staggered microcracks*", Figure 2.8. Nairn also evaluated the evolution of crack density with applied stress for different $[90_m/0_n]_s$ layups, characterised by the same 90° plies thickness and different 0° plies thickness under tensile load [7]. Results are summarised in Figure 2.9, where symbols represented experimental data and lines are empirically fits to the experimental data using the fracture mechanics analysis. Characteristic curves of crack density are quite similar to the $[0_n/90_m]_s$ layup: a rapidly increase of the crack rate at the onset. The increase of 0° ply thickness leads to a delay in terms of transverse ply crack initiation, and laminates with thinner 0° plies exhibit greater final crack density. Results indicated that cracking onset and accumulation depend on 90° ply thickness as well as 0° ply thickness. Comparison between Figure 2.7 and Figure 2.9 revealed the differences in terms of onset and saturation of cracks density between $[0_n/90_m]_s$ and $[90_m/0_n]_s$ laminates, this simulated the same laminate tested in two different directions [7].

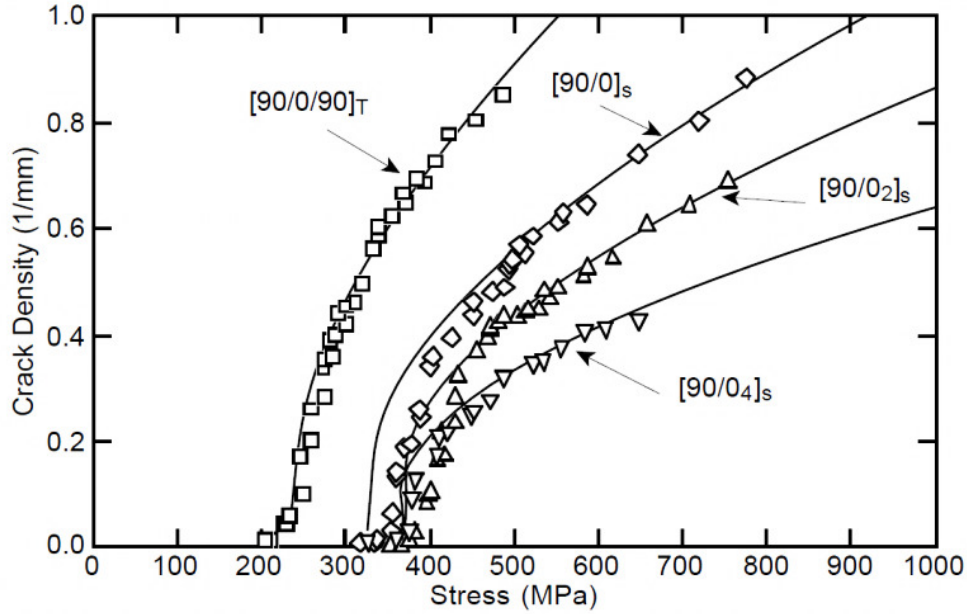

Figure 2. 9 - Microcrack density as a function of the applied stress for carbon/epoxy laminates, characterised by different thickness of the 0° plies. 90° plies thickness was constant. Symbols represent experimental results and lines the data fitting using a fracture mechanics method. Data is from Ref. [14].

At high crack density, curved transverse ply cracks were observed, [13], Figure 2.10. Hu *et al.* [13] explained that curved microcracks occurred only for some in $[0_n/90_m]_s$ laminates, and formed when the crack density associated with straight cracks was larger than a critical value. Curved microcracks were always located near a straight microcrack. One of the consequences of the presence of curved microcracks is, according to [13], a reduction of longitudinal stiffness, while other authors [16] reported that curved microcracks also reduce out-of plane and in-plane stiffness.

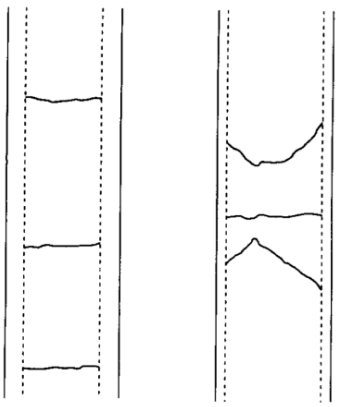

Figure 2. 10 - Location and shape of curved microcracks [13].

Fatigue experiments conducted on cross-ply and quasi-isotropic toughened CFRP [6] suggested slightly different transverse ply crack propagation behaviour with respect to quasi-static loading, where microcrack propagation depends on 90° ply thickness [4, 7]. During fatigue loading transverse ply cracks depend on the 90° ply thickness and also on the amplitude of the fatigue stress. Early works [4] conducted on cross-ply carbon/epoxy laminates showed that transverse ply cracks did not extend across the full thickness of the ply. Increasing the strain, cracks started to extend. It was observed that most cracks initiated in the first few hundred cycles and the rate of new crack initiation decreased as the number of cycles increased. Transverse cracking was observed in fatigue at lower applied stress levels than in quasi-static loading. Delamination did not occur immediately when transverse ply cracks reached the interface, but after a period, called *"incubation period"*. Harrison and Bader [4] suggested this was related to the resin rich region at the interface, which delayed propagation of transverse ply cracks. Nairn [7] explained that during the fatigue loading microcracks depend also on the amplitude of the fatigue stress. In particular, in correspondence to low stress/high cycle fatigue, new microcracks initiate at the specimen edges and propagate slowly through the specimen width (in the 90° ply). Whereas, during high stress/low cycle fatigue, microcracks that initiate at low microcrack density propagate along the specimen width instantaneously, while microcracks that initiate at high crack density, initiate at the edge specimens and propagate slowly along the specimen width.

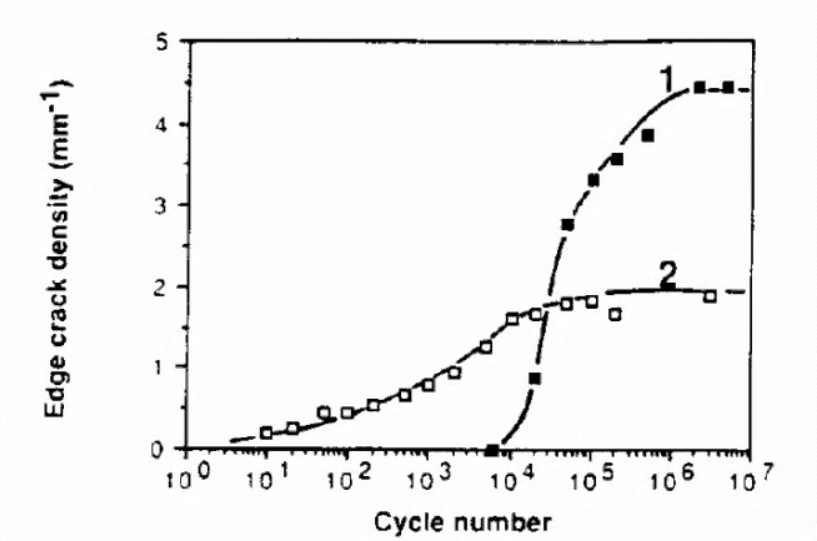

Figure 2. 11 - Microcrack density as a function of number of cycles (linear/logarithmic representation) for two different 90° ply thicknesses: 1 for single layup and 2 for double layup [17].

Lafarie-Frenot *et al.* [17] investigated the influence of 90° plies thickness and stacking sequence in the fatigue loading. Similar results to monotonic loading were obtained. Figure 2.11 shows crack density as a function of number of cycles, for two different layup designed to have a different 90° ply thickness. Overall transverse ply crack density increased with number of cycles. As for quasi-static loading, 90° ply thickness affected the transverse ply cracking onset, propagation and crack density. Thinner 90° plies, represented as number 1 in Figure 2.11, exhibited a delay in terms of transverse ply crack initiation, followed by a sharp increase of crack density formed at the specimen edges, and finally a phase of saturation. Thicker 90° plies resulted in transverse ply cracks initiating at lower numbers of cycles. Crack density was lower than for thinner 90° plies, the propagation was slower with number of cycles, and the saturation value was lower. Figure 2.12 confirms findings for quasi-static loading condition: thinner 90° plies performed better delaying the transverse ply cracks initiation (symbol 1). Indeed, for thicker 90° plies the crack density grows more slowly and the saturation crack density is lower (symbol 2); however, the total crack surface area was significantly higher for laminate with thicker 90° plies (symbol B), as illustrated in Figure 2.12.

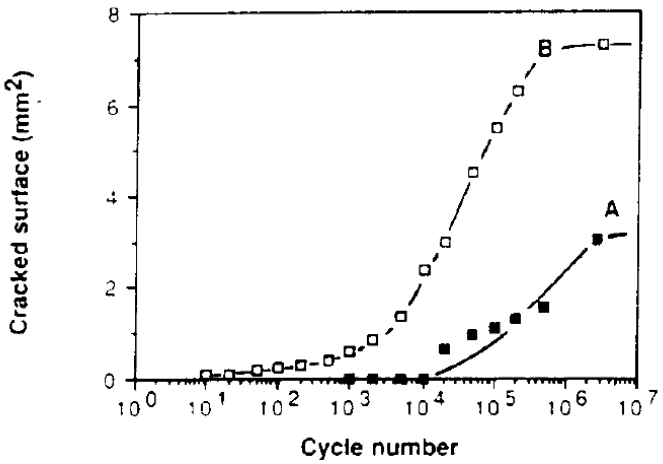

Figure 2. 12 - Cracked surface as a function of the number of cycles (linear/logarithmic representation) for thin (A) 90° ply layup and thick (B) respectively [17].

More recently, Yokozeki *et al.* [6] assessed crack density evolution with number of cycles, identifying three phases: crack initiation, crack growth and crack propagation in the width direction. As the number of cycles increased, edge cracks increased in number without propagation in the width direction. At higher numbers of cycles, edge crack densities

saturated and transverse cracks started to propagation in the width direction. For cross-ply laminates, it was shown that transverse ply cracks grew in the width direction in the same time that other edge cracks initiated. Gamstedt and Sjogren [5] compared micromechanisms in transverse plies in glass/epoxy specimens for two different loading conditions: tension-compression and tension-tension fatigue. Tension-compression fatigue resulted in more rapid damage accumulation than tension-tension fatigue. The underlying mechanism was a more rapid debond growth around the fibre in tension-compression loading. However, most fatigue tests were conducted under tension-tension cycling by various authors, due to difficulties such as buckling phenomenon associated with tension-compression fatigue loading.

2.2.2 Longitudinal splits

'Splits' are matrix cracks generate in the loading direction and run parallel to the fibre direction, and for that reason are also called 0° ply cracks. They are detected for both quasi-static and cyclic loading. Early works [18] attributed the nucleation of 0° splits to the presence of local shear stress, but subsequent studies [19] confirmed that split initiation is affected by a combination of shear stresses and transverse stresses. Nevertheless, once splits appear, researchers are agreed that propagation is dominated by shear stresses. Daken *et al*. [18] tested notched carbon/epoxy specimens under tension-tension cyclic loading: results indicated that splits occurred from both side of the notch, and neither initiated simultaneously nor propagated with the same rate growth. They defined different combination possibilities for split initiation around the notch, as shown in Figure 2.13.

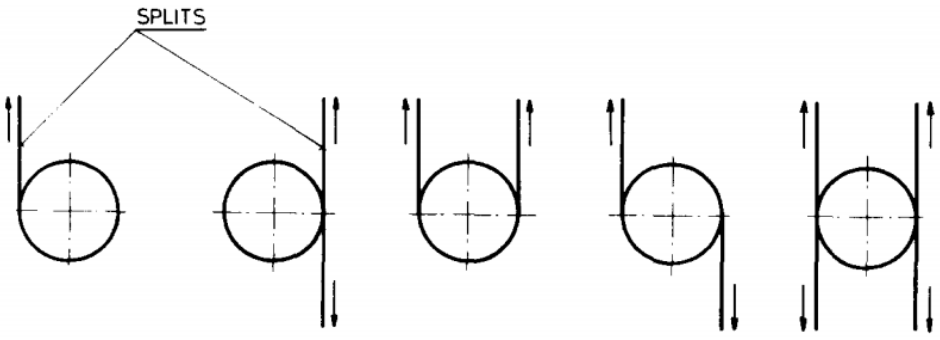

Figure 2. 13 - Modes of split initiation [18].

The trend of the split length as a function of the number of cycles (in a semi-logarithm graph) appeared linear. This observation was contradicted by Spearing *et al*. [20], who studied the damage developed in notched carbon/epoxy laminates under quasi-static and cyclic loading. Spearing *et al*. [20] observed that under quasi-static load, split length increased linearly with increasing load, Figure 2.14 (a). However, fatigue test results for split length showed points, which did not fit a linear distribution, Figure 2.14 (b).

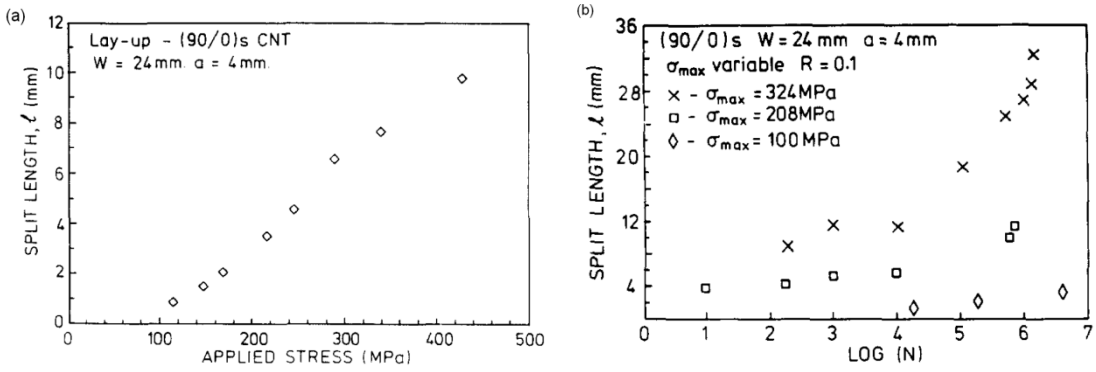

Figure 2. 14 - Split length as a function of maximum load for monotonic load (a) and as a function of number of cycles for fatigue (b) for three different maximum load. Notched carbon/epoxy specimens used with a layup of $[90/0]_s$ [20].

Furthermore, they demonstrated that split growth depended primarily on the notch size but not on the notch shape. Fibre breaks were observed along the propagation of 0° splits and at the intersection between 0° splits and transverse ply cracks. The influence of laminate thickness Figure 2.15 (a) and the influence of ply thickness Figure 2.15 (b) on split growth was also evaluated. Split length, l, was normalised with notch length, a.

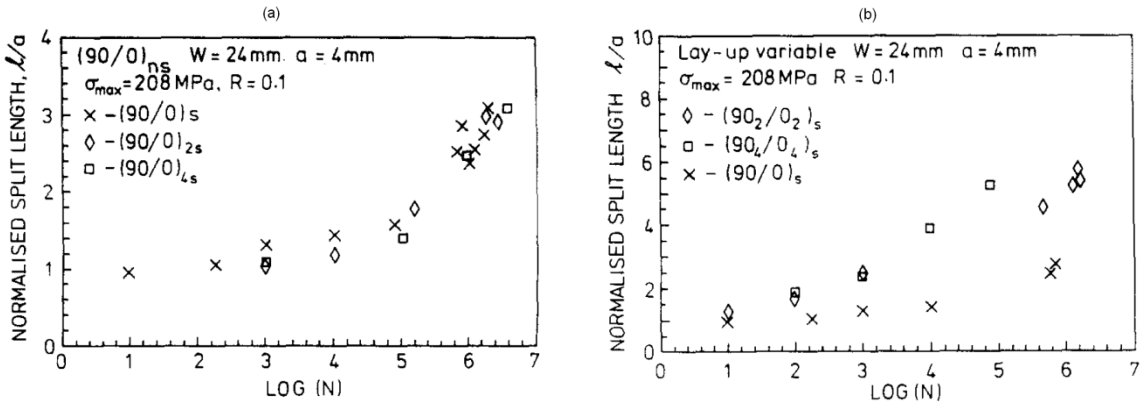

Figure 2. 15 - Influence of laminate thickness (a) and ply thickness (b), respectively [ref 22].

Overall laminate thickness had little affect on the evolution of normalised split length, whereas the thickness of plies had a greater influence. In particular, normalised split lengths increased for increasing ply thickness, Figure 2.15 (b). Spearing and Beaumont [20] also compared notch damage for monotonic and cyclic loading and concluded that damage grew in a self-similar manner for both loading regimes. Recent studies, obtained by Moffat *et al*. [21], on current-generation, particle-toughened, graphite-epoxy laminates investigated the microstructure of splits under quasi-static loading for carbon/epoxy specimens. Their results revealed that 0° ply cracks are not planar and grow in a different manner in resin-rich and fibre-rich regions. In particular, splits appear as hackles or echelon cracks in resin rich region with some bridging (due to both toughening particles and resin) between them. In fibre-rich region splits were smooth and straight, due to probably debonding of the fibre-matrix interface. Some fibre misalignment throughout the ply was observed but few individual fibre breaks apparently occurred due to fibre misalignement.

2.2.3 Delamination

Delaminations are cracks at the interface between plies with different orientation and may significantly reduce stiffness and strength of the material, often contributing to the failure of the component. Delamination can appear under static loading, and cyclic loading. Johannesson *et al*. [22] identified three steps in delamination development of angle-ply carbon/epoxy specimens: fibre debonding at the beginning, attributed to stress concentrations at the interface; cracks formed in the resin region, and finally debonded regions and resin region cracks linked together by the formation of microscopic cracks. They supported the theory, according to Pipes and Pagano [23], that delamination occurred due to normal tensile stresses and shear stresses. Recently Greenhalgh *et al*. [24], studying the delamination failure for a carbon fibre/epoxy composite, attributed delamination to a combination of different micro-mechanisms by which delamination migrated, determining the growth process. The propagation process grew parallel to the upper or lower ply at the interface, which ply depending on the orientation of the interlaminar shear.

The fracture surfaces of delaminations have been observed by different authors over the years in order to identify the underpinning mechanisms. Johannesson *et al*. [22] carried out tension tests on carbon/epoxy and studied the fracture surface. They identified two preferential paths for initiation and propagation of delamination cracks, one along each side of interlaminar regions. Observations showed small amounts of fibre pull-out on the fracture surface, and

that the surface between the fibres was smooth. They identified two features that characterized delamination fracture surfaces: debonded fibres and resin failure in the form of serrations, which were mainly present in the outer parts of the plies adjacent to the interlaminar resin rich region. Serrations were described as the result of microcracks with their planes perpendicular to the tensile major principal stress, Figure 2.16.

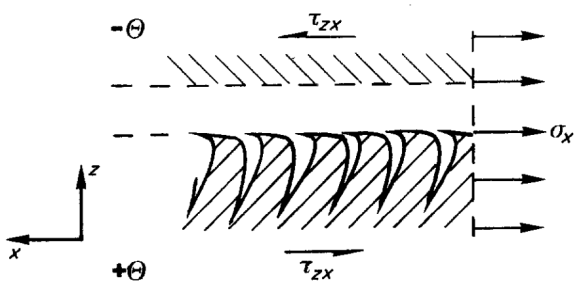

Figure 2. 16 - Schematization of serrations [22].

Reeder [25] took into account three different composite materials, a brittle graphite/epoxy, a toughened graphite/epoxy (consisted of an epoxy matrix with thermoplastic additive), and a tough graphite/thermoplastic. An insert at the midplane of the specimen was used to promote delamination development. SEM photomicrographs showed that the fracture surface changed with material considered and mostly with the different mode established. In order to create mode I opening in the specimen double cantilever beam tests were performed (DCB) and to produce mode II shear load, end notch flexure (ENF) was utilised.

However, in reality, delamination develops under a combination of mode I and mode II (mixed mode). Reeder [25] performed mixed mode bending tests (MMB), as a result of a combination of DCB and ENF. Results demonstrated that for brittle graphite/epoxy under mode I, the fracture surface was flat, indicating a brittle cleavage fracture. Under mixed mode loading, the fracture surface became rougher. Fracture surfaces of toughened epoxy were very similar to the brittle epoxy in terms of failure mechanisms. In contrast, the fracture surfaces of the thermoplastic composite were noticeably different from that of the epoxy. In particular, all fracture surfaces contained “cusps”, attributed to the yielding of matrix. Ridges and valleys were also observed for thermoplastic composite. The fibre pulled-out of the valleys caused ridges. In this last condition, different mixed mode ratios created different cusps orientations.

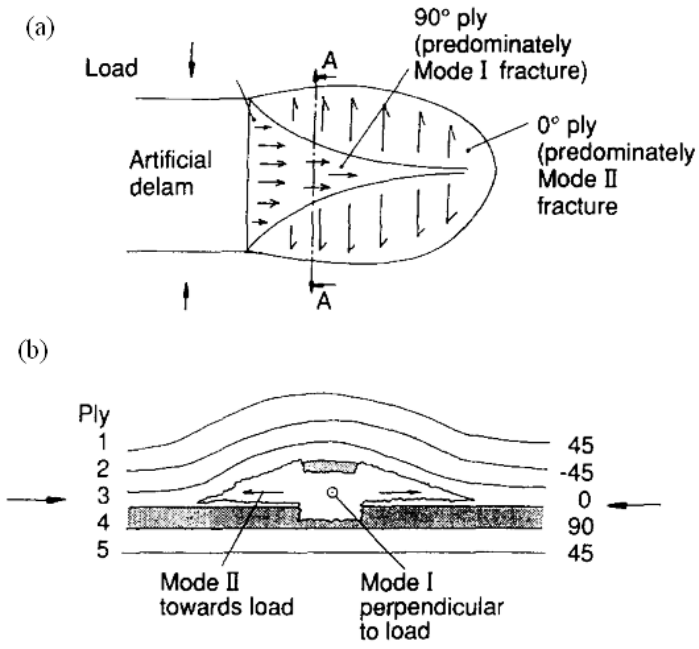

Figure 2. 17 - Schematization of delamination growth (a) and cross section A-A (b), [26].

Greenhalgh investigated delamination growth under quasi-static compressive loading in carbon-fibre epoxy [26] using an insert coupon between two adjacent interfaces for a foam filled panel with layup $[(+45,-45,0,90)_3]_s$, and for a coupon with layup $[(+45,-45,90,0)_3]_s$, fitted with an anti-buckling rig. Greenhalgh [26] noted that delamination grew in two planes: from one side of the insert, it was predominantly mode I, whilst on the other side of the insert, it was mainly mode II, as shown in Figure 2.17. Initial growth was, predominantly in mode I, but the mode II extended over a greater area than mode I. He also explained the mechanisms of delamination growth, as a combinations of two factors, one was compressive stress parallel to the loading axis, which tended to close the crack reducing the bending movement and leading to predominantly mode II loading; the other was the tensile stress in delamination plies, perpendicular to the applied loading, due to the out of plane deflection and to the lateral Poisson expansion, which led to establishment of mode I loading in the same direction as the applied bending load. Delamination resulted to be independent of the initial defect size. Gilchrist and Svensson investigated delamination fracture surfaces in carbon/epoxy under static and fatigue conditions [27]. They used an artificial non-adhesive starter delamination along an interface to simulate delamination. Results of their experiments were divided in terms of loading mode generated in the specimens. For mode I, fracture

surfaces appeared smooth with ridges, valleys and few fibre breaks. Fibre pull-out and lack of cusps were the dominant features of the mode I fracture. Fatigue surfaces under mode I loading were very similar to those created by quasi static mode I [27], without cusps or striations and with the addition of significant resin debris**.** Static mode II was characterised by rough resin fracture, debris, nodules, and cusps. Mode II fatigue fracture surfaces featured large amounts of debris, loose nodules in the resin between fibres, and no striations. More broken fibres were observed in fatigue than in quasi-static mode II loading. Mixed mode loading resulted in damage that was a combination of that caused by independently applied mode I and mode II. This was confirmed by the observation in static loading of occasional fibre pull-out with resin remaining attached to the fibres. Very small cusps were observed around the sites of pulled-out fibres, ridges and valleys. Resin debris and nodules were present in large amounts for fatigue loading, together with some shallow cusps. There was not the presence of cusps for mode I [27]. This observation results in contrast with that of Reeder [25], who detected cusps also in mode I for thermoplastic composites. Greenhalgh *et al*. [24] observed that changes in morphology reflected changes in the fracture processes. These changes were explained by considering the resolved tensile stress, as a combination of shear and peel stresses, as shown in Figure 2.18 (a). Under mixed mode or mode II loading, resolved stress and consequently the crack front, was oriented out of the laminate plane; therefore delamination propagated out of the defect plane and migrated upward. In the specific case that the delamination path migrated towards a ply, in which the fibres were aligned with the normal to the delamination front, the delamination remained within the defect plane as shown in Figure 2.18 (b). Conversely, if the ply orientation was not aligned with the normal to delamination front, ply splitting developed, and consequently the delamination migrated into the next ply interface Figure 2.18 (c).

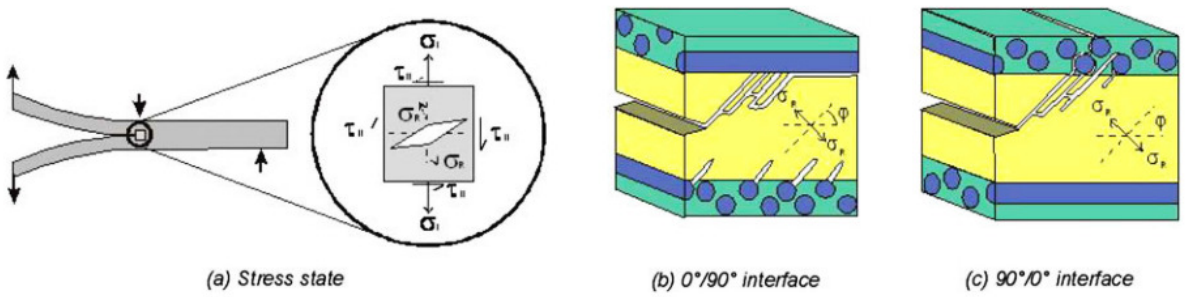

Figure 2. 18 - Stress state at the tip of delamination under mixed-mode loading (a), delamination mechanisms at the interface (b), (c), [24].

Greenhalgh *et al*. [24] established that delamination migrated through the laminate until it reached an interface in which the ply was oriented parallel to the driving force, and identified migration as the main factor that controlled delamination growth, and that it was more important than initial defect shape and size.

2.2.4 Fibre breaks

Fibre breaks occur in composite materials under static and fatigue load, for different level of loading. In particular, for low loads isolated fibre breaks spatially distributed [28] and fibre breaks along 0° splits [21] were observed in carbon/epoxy toughened cross-ply specimens; whereas at high load, formation of clusters of broken fibres was seen [28, 29]. Nevertheless, the mechanics of cluster growth are not well understood, Scott *et al*. [28] observed a cluster of 14 fibre breaks for a load equal to 94% of the failure stress, but at the previous load step (88% of the failure stress), the same cluster had not appeared. Relations between fibre breaks and other composite damage were analysed, but a clear correlation was not found, and different layup showed dissimilar behaviour. For instance, Scott *et al.* [28] did not find correlation between location of transverse ply cracks and fibre breaks in the 0° ply, for a particle toughened carbon/epoxy cross ply laminate. Conversely, Wright *et al*. [30] using an untoughened quasi-isotropic carbon/epoxy, observed a concentration of fibre breaks at the -45/0 interface, aligned with the split in the - 45 ply.

It is well known that the strength of composite is not exactly expressed by rule of mixtures, due to the fact that fibres have stochastic strength distributions. The variability of fibre strength is affected by the distribution of flaws in the fibres, cluster formation and composite failure are influenced by the load redistribution in the neighbouring fibres around the fibre breaks, which have to be taken into account. The most widely used model to describe fibre strength distributions is Weibull statistics. Pickering *et al.* [31] found agreement between the numbers of fibre breaks observed experimentally with the Weibull statistical fit. However, recent studies conducted by Scott *et al.* [28] underlined the presence of clusters of fibre breaks and consequently the importance of load sharing, demonstrating that Weibull distribution appears not appropriate on its own to describe fibre failure development in composites.

Different approaches were used to predict fibre failure, among these, Equal Load Sharing proposed by Rosen [32] models unidirectional composite ply as a chain of short bundles, in

which all fibres share the applied load equally and the broken fibres do not carry load. The Global Load Sharing approach is based on the concept that load in a fibre depends on the proximity of the nearest fibre breaks [33]. Individual fibres usually are modelled using the "weak link" principle, considering fibres as a chain of short segments with failure occurring at its weakest point when the fibre strength exceeds its local failure strain. Marston *et al*. [29] studied unidirectional carbon/epoxy composite tows subjected to axial load. They established that the number of fibre breaks increased exponentially with the increasing of load. Similar results were showed by Scott *et al*. [28], who fitted experimental data with a power law for breaks within 0° plies. Studies conducted to date have been aimed to assess stress and interfacial shear stress along fibre breaks, stress distribution along neighbouring fibres, understanding the influence of the stress concentration factor due to fibre breaks under axial load.

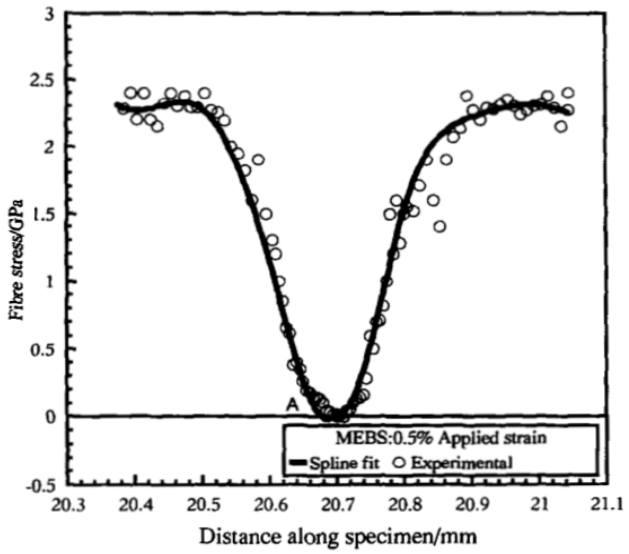

Figure 2. 19 - Fibre stress along fibre breaks [29].

Marston *et al*. [29, 34] using the laser Raman spectroscopy evaluated the stress along a single broken carbon fibre in an epoxy matrix for a tow subjected to axial load, as represented in Figure 2.19. The lowest point, where the fibre is stress-free, corresponds to the point of failure, and the stress builds up to the far field value over a distance of approximately 200 µm either side of the break. The fibre stress dropped from zero at the tip of the broken fibre to a maximum value in correspondence of a distance, called ineffective length, which resulted 200 µm for single fibre and 220 µm for a fibre in a composite tow.

Value of ineffective lengths measured by Scott *et al*. [28], for a carbon/epoxy laminate, were in the range between an upper bound of 335 µm and a lower bound of 70 µm, with an average of 150 µm. The interfacial stress distribution has been also calculated [29, 34] along fibre breaks for single fibre breaks in a composite tow as shown in Figure 2.20. Results showed a minimum value of zero shear stress at the fibre break that increases until it reaches the maximum value and drops again to zero over the ineffective length.

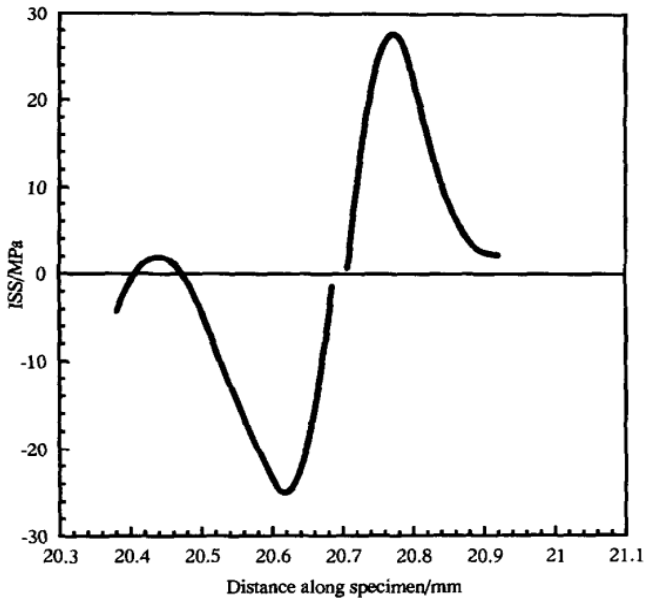

Figure 2. 20 - Interfacial shear stress along the fibre breaks, for a single broken fibre in a composite tow [29].

The interfacial stress distributions in neighbouring fibres due to fibre breaks were also evaluated [34]. Considering two fibre breaks, interfacial stress resulted greater than the case of one fibre breaks, and exactly double. The tensile fibre stress distribution along the neighbouring fibres shows a corresponding increase in stress around the fibre break, as shown in Figure 2.21. According to Marston *et al*. [29] stress concentration coefficient was defined as the ratio between the axial stress in a fibre adjacent to the broken fibre and the stress intensity. They attributed the fibre break stress concentration factor directly related to the matrix and fibre properties, inter-fibre distance, number of broken fibre, and ineffective length. When the fibre breaks, the stress is transferred to the neighbouring fibres, consequently the stress concentration factor should be greatest in the nearest fibre, and when a cluster of fibre breaks is formed, the stress coefficient factor increases.

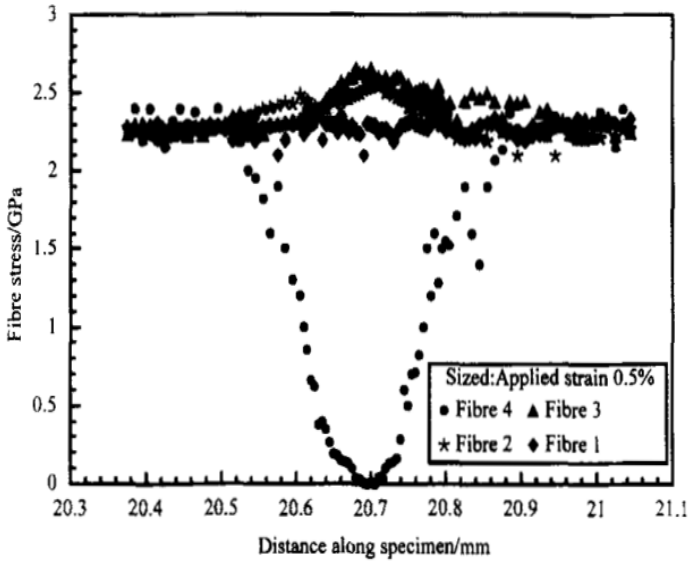

Figure 2. 21 - Fibre stress distribution along fibre breaks (Fibre 4) and the neighbouring fibres (Fibre 1,2,3) for a composite tow [34].

In particular, Marston *et al*. [29] found experimentally a stress concentration factor of 1.18 in the nearest neighbouring fibre for single fibre breaks, and Pickering [31] using numerical model predicted 1.07. These values are smaller than that calculated previously by Hedgepeth [35], using a shear lag method, which was found to be 1.33 for a fibre neighbouring a single fibre break. The difference probably is due to the fact that Hedgepeth did not take into account the inter-fibre distance and the fact that load is shared by all the neighbouring fibre and not only by the nearest. Hedgepeth [35] also predicted, using theoretical analyses, the stress concentration factor for dynamic loadings by an amplification coefficient. Results showed a significant increase of the stress coefficient factor for dynamic load respect to the uniaxial load on the same fibre neighbouring. The model estimated a dynamic stress coefficient factor of 1.53 for single fibre breaks against 1.33 for static load and a dynamic stress concentration factor of 2.19 for the nearest fibre to a cluster of three broken fibres, against the value of 1.83 for static loading [35]. No experimental studies on the micromechanics of fibre breaks under fatigue loading have been conducted.

2.3 Modelling fatigue damage

There has been great effort by researchers to develop methods for modelling fatigue damage and to predict the fatigue life of polymer composites. To date no model exists that predicts

fatigue life and residual strength accurately for composite materials. In this section some of the models that have been proposed are briefly reviewed.

Various methods for model classification have been used with the aim of allowing comparison between modelling approaches. In this section a classification is followed, this divides the available models into three main categories in order to facilitate discussion: damage accumulation, models based in most cases on experimental stress-life curves (S-N); phenomenological models, such as residual strength, and residual stiffness models, based on modified material properties due to damage accumulation; and micromechanics models, based on the inspection of local damage directly. However, this distinction is not rigid, and some methods may be placed in more than one category, because they use more than one approach at the same time.

2.3.1 Damage accumulation models

Fatigue damage accumulation models are based on the calculation of a non-dimensional damage parameter, D, which expresses the amount of life that the composite has already spent. In most models, D=0 at the initial stage and 1 when failure is reached. These models usually need only S-N curves for calibration and do not take into account the physical damage state. The earliest such method was formulated by Palmgren-Miner for metal alloys [36], also known as "Miner's rule", in which the accumulation of damage was described by a linear damage accumulation rule. The Palmgren-Miner model has been found to be inaccurate for composite materials. Many variations of such linear damage accumulation models have been proposed. Owen and Howe [37] introduced a damage accumulation model based on observations of crack development. Owen and Howe model is linear and consisted in a modification of the Palmgren-Miner linear accumulation damage rule using two parameters that are obtained by fitting the experimental data. Hashin and Rotem [38] developed a model of damage accumulation for homogeneous materials, and since it is general, this was considered also for composites. They developed analytical damage equations based on the assumption that damage develop in a similar way of S-N curves. Hashin and Rotem's method is phenomenological, and includes no physically observable damage mechanisms.

2.3.2 Residual strength models

In residual strength models the failure criteria is described in terms of residual strength, in relation to the maximum stress. Life predictions are dependent on the current load and consequently on the damage. All residual strength models are based on the assumption that residual strength decrease monotonically with the increasing number of cycles, the initial fatigue strength is equal to the static strength, and failure occurs when the residual strength equals the maximum applied stress [39]. Davis *et al*. [2] specified that residual strength models are also based on one or both of these hypotheses: the statistical variability of static residual strength may be described using a Weibull distribution; residual strength of fatigue loading in correspondence of a fixed number of cycles can be related to the static strength using a deterministic equation.

Schaff and Davidson [40, 41] applied a phenomenological residual strength model. Phenomenological models characterise residual strength as a function of macroscopic properties. Due to this reason, a large experimental data set is required to deduce the model parameters. In addition, this approach results strictly dependent on the properties of a specific material and on the loading condition, and it is very difficult to obtain a generalization valid also for other situations. Schaff and Davidson's models are based on the assumption that the distribution of fatigue life and residual strength can be modelled using Weibull distribution.

An interesting peculiarity that they found was the observation that in some cases, the application of repeatedly changing load levels resulted in more damage than the application of the same load levels in longer "blocks" . They called this the "cycle mix effect" [39] and to take into account of this situation they introduced a factor to reduce the residual strength whenever the magnitude of the mean stress increased. The predicted residual strength after fatigue, under constant amplitude, agreed well with the experimental results [40].

Adams *et al*. [42] developed an empirical model to predict residual strength for constant amplitude fatigue loading. They reported the dependence of strength on the stress level, Figure 2.22 shows how high load cause an early residual strength drop, as expected. The initial residual strength showed apparent fluctuations inside the scatterband, this was ascribed to the off-axis plies and fibre misalignment along the 0° plies, which were re-oriented under the tensile loading.

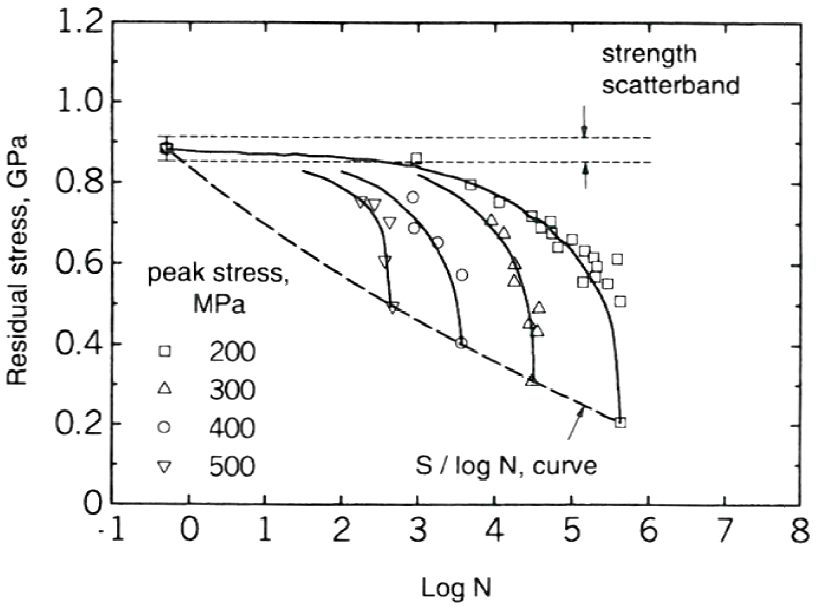

Figure 2. 22 - Residual strength in fatigue loading for various maximum stress, according to Adams [42].

Reifsnider and Jamison [43], described fatigue damage in terms of critical elements, responsible for controlling failure, and sub-critical elements, failure of which do not determine overall laminate failure. Therefore, degradation of sub-critical element does not have a major effect on the residual strength of laminate. They attributed this to the internal stress redistributions when a sub-critical element fails, and the overall redundancy in load paths through the material (and structure). Reifsnider and Jamison [43] also identified three stage of fatigue damage: an initial stage of rapid degradation, a second phase in which the damage slope decreases and a final part, in which the damage rate increases again and leads to failure, Figure 2.23. They made the assumption that residual strength followed a similar trend [39]. Moreover, their model was able to predict the first two stages or the last two stages, but not all stages at the same time. Spearing and Beaumont [44] developed a method to predict post fatigue strength for carbon/epoxy notch specimens, subjected to tension-tension cycling. Residual strength was modelled as a function of loading condition, specimen geometry and lay-up. They noted that fatigue damage and quasi-static damage were characterised by the same components, thus used the same parameters to model both loading cases. Another approach proposed by Hahn and Kim [45] used a correlation between static strength and fatigue life distributions. This was later termed the "strength-life equal-rank assumption" (SLERA) by Chou and Croman [46].

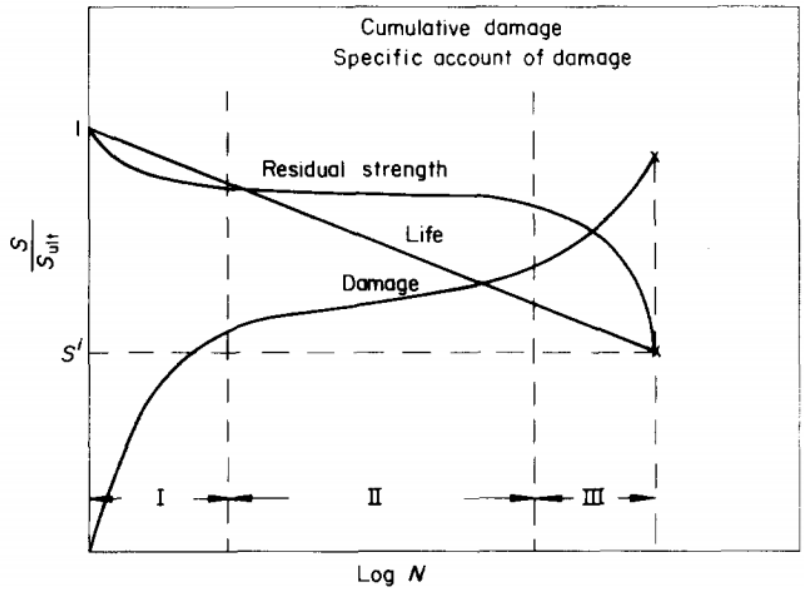

Figure 2. 23 - Schematization of the damage, residual strength and lifetime in composite laminates [43].

Hahn and Kim [45] assumed that there was a one to one relationship between the statistical distribution of the residual strength for static loading and for fatigue loading. As a consequence, a specimen of a certain rank in the fatigue life distribution would be equivalent in strength to a specimen of the same rank in the static strength distribution. They also introduced the concept of the rate of change in residual strength, characterised using a power law, without take into account damage mechanisms. SLERA proved to have some limitations: firstly, is not possible to measure the initial strength and fatigue life using the same specimen, because both tests are destructive; secondly, is not possible to apply this approach to notched specimens or impacted specimens, because the failure mechanisms are different between static and cycling loading for these loading conditions [2, 39].

2.3.3 Residual stiffness models

Residual stiffness models are based on the acquisition of stiffness reduction due to load application. Some of these models are based on the assumption that residual stiffness decrease monotonically as the number of cycles increases. In early studies, Beaumont and Harris [47, 48] found that for unidirectional high-modulus carbon fibre-reinforced plastics, there was a not significant change in stiffness until failure. However, a different behaviour was observed for cross-ply laminates, in which the presence of transverse ply cracks caused a

reduction in stiffness commencing from the first cycles. The advantage of residual stiffness models with respect to residual strength models, consists in the possibility of estimating the remaining life using non- destructive techniques. Spearing and Beaumont [49] predicted the stiffness of notched cross-ply laminates. Their model includes a combination of experimental and theoretical results, which were incorporate in a finite element representation to predict stiffness. The effect of transverse ply cracks was taken into account by degrading the elastic constant of the transverse plies in a specific region. The model was able to predict the effect of damage propagation on stiffness for different laminates; however it requires *a priori* knowledge of the damage propagation path and sequence as an input to the model. Reifsnider *et al*. [50] found that stiffness change may be related to the fatigue life and residual strength using models based on micro-damage observation. As well as in their model to predict residual strength, also in this of stiffness reduction, they distinguished between critical and sub-critical elements. Fatigue life was defined considering changes in stiffness in sub-critical elements (matrix), and changes in strength in critical elements (fibres, 0° plies). They also included in the model the influence of the fibre-matrix interface, considering the degradation at the interface fibre-matrix by an interfacial efficiency; an equation obtained using experimental data, which is function of the number of cycles.

2.3.4 Micromechanics models

Micromechanics models characterize damage at the local level and thus determine the strength, stiffness and life of the laminate. However, in continuous fibre composites the damage assumes different aspects (transverse ply cracks, delamination, fibre breaks, splits and so forth) that are also spatially distributed and interacting with each other. Therefore, development of a micromechanics model is complex. Many researchers have tried to do this, using numerous approaches to the problem. Sometimes researchers have tried to restrict the various damage modes, considering only a predominant damage mechanism. For instance, matrix microcracking has usually been modelled as small cracks parallel to the fibres and delamination modelled as a single crack [2]. O'Brien *et al*. [51] developed a method to predict life for composites subjected to tension fatigue that incorporated fracture mechanics of delaminations and their effect on composite fatigue life. The main damage mechanisms identified were matrix cracks and delaminations, and this was shown to cause a reduction in laminate stiffness. The amount of stiffness depended by many parameters, such as laminate

lay-up, ply orientation, cracks density, relative modulus of fibre and matrix. However, to predict stiffness loss as number of fatigue cycles, there was the need to characterise the damage onset and propagation by a parameter, which resulted independent of laminate structural variable. This was achieved using the strain energy release rate G, associated with the aforementioned damage. Researchers in many models have used this parameter. O'Brien *et al*. [51] considered the influence that microcracks and delaminations had on G, in an independent manner. In other hands, they did not take into account the reciprocal interaction between the two damage modes. Therefore, this approach results to be adequate when there is a predominant damage mechanism. General applications with interacting modes become more difficult to characterize in terms of energy release rate. Song and Otani [52] predicted fatigue life for a cross-ply laminate, evaluating microdamage measurements, such as transverse crack density; fibre fracture crack density and delamination crack density by an optical microscopy. They found that fatigue failure occurred due to residual strength of each layer and interlayer, which decreased exponentially in function of the crack densities. Results showed good agreement with experimental data. Dzenis [53] characterized damage for low cycles, he applied a triangle wave and monitored damage by acoustic emission, finding that the most damage initiated and propagated under the loading part of the cycles. He also used to predict failure a "stochastic mesomechanics" [54] approach, which combined the laminate theory and theory of stochastic processes. In this way, the model results able to take into account the randomness properties of the composite, laminate microstructural parameters and the loading. The application required statistical distributions of the ply stiffness and strength properties. This approach seems promising due to the opportunity to follow damage cycle by cycle, however Dzenis characterised his work only for few cycle, less than 20, and it is unclear how the model should work at high number of cycles. Other models have been developed for fatigue loading based on a continuum mechanics foundation, called as "continuum damage mechanics" (CDM), which incorporate the effects of damage induced in stiffness or other characteristic properties, in the constitutive equations. Damage variable in these models are represented by tensors of various orders, such as scalars, vectors or tensors. Laws *et al*. [55] developed one of the first CDM. He used a scalar damage parameter, based on matrix crack density, and introduced this on the constitutive equations, to model the material stiffness. In a similar way, Talreja defined a damage vector, based on matrix cracking [56], including later also the delamination effect [57]. Allen *et al*. [58, 59] based their model characterizing damage by a second-order tensor depended of measures of damage to model stiffness degradation.

Finite Element Analysis approaches have been used to model fatigue damage in composites, employing a number of varying techniques. These models generally applied stiffness reduction of elements, properties reduction of elements that fail, cohesive element to model the neighbourhood of crack initiation and propagation [39]. Due to micro-scale modelling, in most cases it is not possible to model the entire composite specimen using the computational platforms available. In order to overcome this issue, some authors applied the concept of 'representative volume element' (RVE) [60] or, similarly, the concept of 'repeated unit cell' (RUC). This assumption allows moving the representation on an equivalent fibre-matrix volume, with consequently advantages in terms of computational efforts. Shokrieh and Lessard [61] presented a numerical modelling of fatigue behaviour in composites, called 'progressive fatigue damage model', based on stress analysis, failure analysis and material property degradation rules. The material properties of elements are degraded using an analytical technique. Model allowed simulating cycle-by-cycle composite behaviour under fatigue loading. Results showed reasonable agreement with experimental data.

2.3.5 Conclusions on fatigue modelling

The preceding discussion on fatigue damage modelling highlights the difficulty associated with modelling fatigue behaviour and predicting the lifetime of composites. Many complications emerged due to their typical complexities, such as the interaction of various damage with each other, scatter of fatigue data, dependence of loading condition and laminate properties, which sometimes lead to obtain a model valid for only one specific combination of the aforementioned parameters. These and other factors did not lead to have a reasonable criterion that allows life prediction in composite materials, despite the efforts by researches and the various approaches followed. Today, the most promising way seems to be the computational modelling, even though the efforts in this direction are 'relatively recent'; related to the improvement to computational platforms. However, among the aforementioned models, only few are physically based. Physically based models are desirable because they are directly related to the damage mechanisms and allow to give a real interpretation of the phenomena, seeking to assess the correlation between fatigue life and damage failure mechanisms under cycling loading. The requirement to understand damage mechanics on fatigue life is the main thing to be able to use composite materials.

Chapter 3 X-Ray Computed Tomography

3.1 Introduction

Tomography represents the evolution of the traditional radiography, in which structures appear superimposed due to the projection of all the information into a two-dimensional imaging plane. Consequently the main limitation was the reduced visibility [62]. Developed initially for clinical applications, recently X-ray computed tomography has gained considerable interest in areas such engineering science, biomedical science, archaeology, and palaeontology. This technique is used as a generic diagnostic tool for non-destructive material testing and three-dimensional visualization. Techniques and methodologies are explained in this section from an intuitive perspective, without use their mathematical formulation, which can be complex.

3.2 Physical Principle

As X-rays penetrate an object, depending on the particular paths, X-rays are attenuated to varying extents. Measuring the absorption for various angles of rotation is possible to reconstruct the object from the projections. Figure 3.1 illustrates this principle, where $p_{\gamma i}$ represents the attenuation profile of the beam versus the X-ray detector under a particular projection angle γ_i. If different attenuation profiles are plotted over all angle of rotation γ_i, a projection integral value is obtained [63].

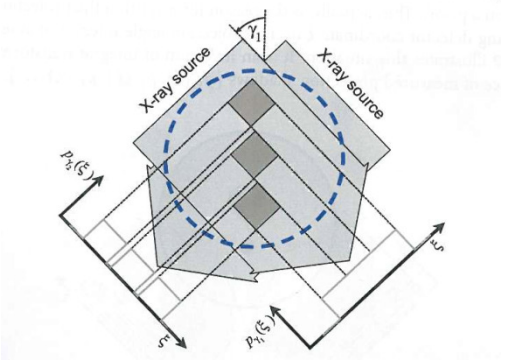

Figure 3. 1 - Schematic illustration of computed tomography for three objects under the projection of two angles [63].

X-rays are known to have a high, material-dependent capability to penetrate matter. However, the radiation intensity decreases exponentially while running through an object along the incident direction. This attenuation is due to absorption and scattering. The most important physical mechanisms of X-ray/matter interaction are: Rayleigh scattering, Compton scattering, photoelectric absorption, and pair production.

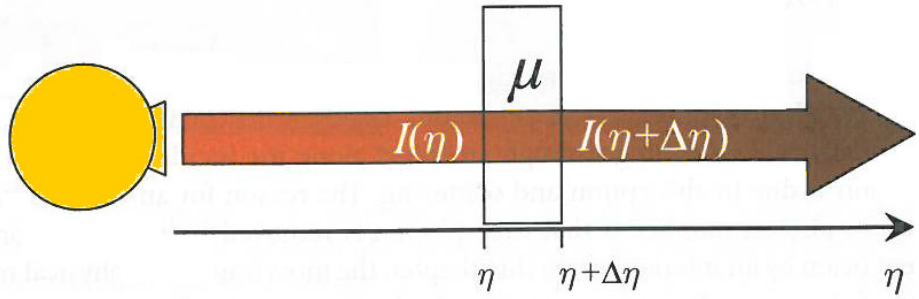

Figure 3. 2 - Model of monochromatic x-ray attenuation within a homogeneous object [63].

All mechanisms that lead to a coefficient of attenuation of radiation intensity are incorporated in a single attenuation coefficient. Assuming a monochromatic X-ray beam, the X-ray intensities measured on the entrance and exit sides of a uniform material (Figure 3.2), follow the Beer-Lambert law:

$$I(\eta) = I_0 e^{-\mu\eta} \tag{3.1}$$

In this equation, I_0 is the entrance X-ray intensity, I is the exit X-ray intensity, η is the thickness, and μ is the linear attenuation coefficient of the material. The linear attenuation coefficient is an additive combination of a scatter coefficient, μ_s, and an absorption coefficient, α.

$$\mu = \mu_s + \alpha \tag{3.2}$$

In general, μ changes with the X-ray energy and with different materials.

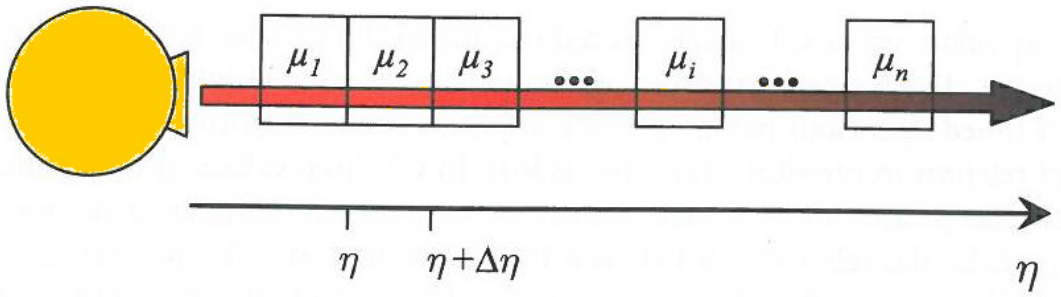

Figure 3. 3 - Attenuation of X-ray through a non-homogeneous object [63].

When an object is not uniform and there is spatial variation in attenuation, Figure 3.3. Assuming $\Delta\eta$ approaches zero, the solution for the intensity attenuation after a running a material length L is given by:

$$I(L) = I_0 e^{-\int_L \mu(\eta)d\eta} \tag{3.3}$$

The index of the exponential term represents the projection measurement in fixed direction. Buzug [63] reported a schematization, after Laubenbenger and Laubenbenger [64], of the attenuation value as a function of wavelength of incident beam, atomic number, mass density, and thickness of the medium, Figure 3.4.

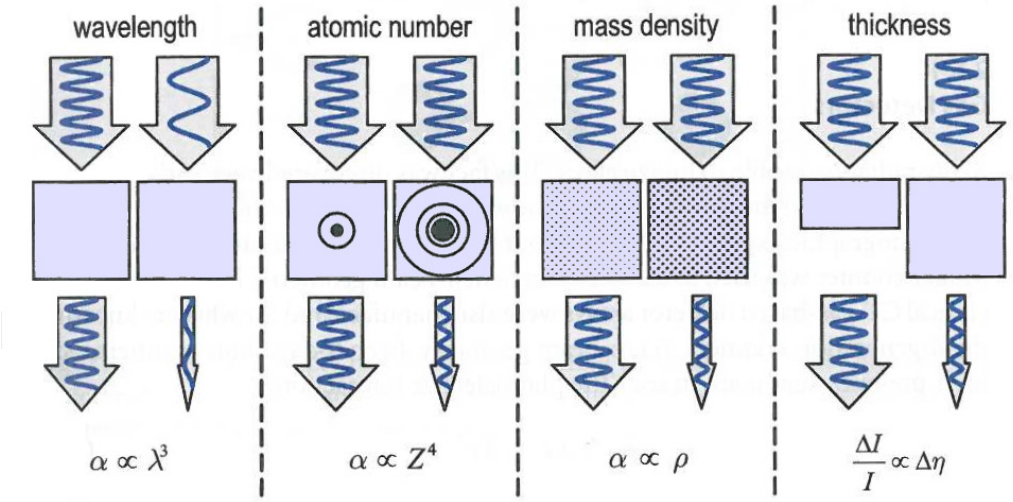

Figure 3. 4 - Attenuation as a function of wavelength of incident beam, atomic number, mass density, and thickness of the object, respectively [64].

Given that the relationship between X-ray absorption and the density (Figure 3.4) is known, other parameters, including the 3D internal structure can be obtained from the projections. The object is typically rotated thorough an angle of 180°.

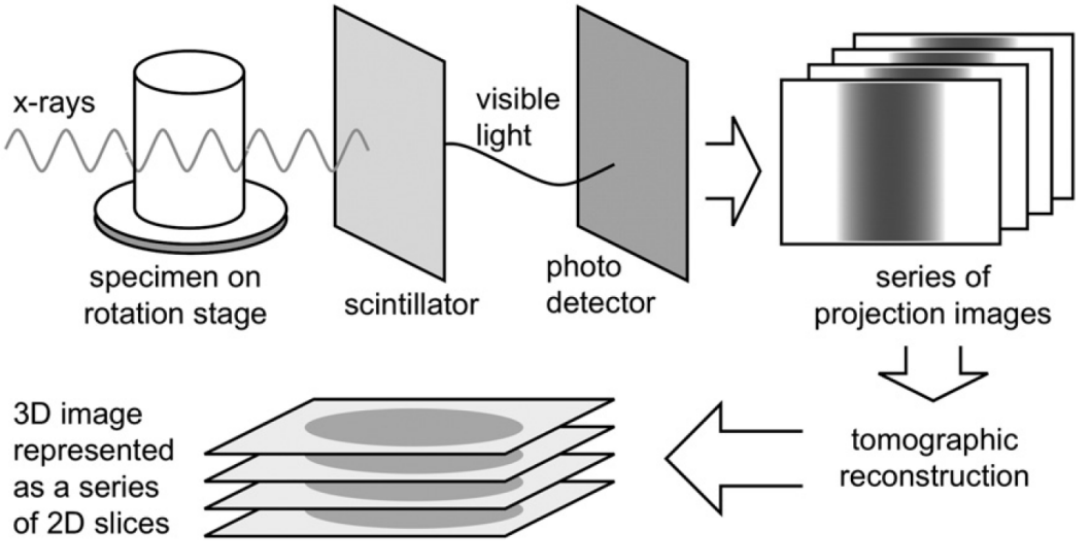

Figure 3. 5 - Schematisation of X-ray Computed Tomography acquisition and reconstruction to produce a 3D map of X-ray absorption in the volume [62].

During the rotation, the attenuation of X-ray beam is measured in a finite number of angular increments. Tomographic reconstruction is performed by an inverse Radon algorithm. Resulting 3D volume is shown as a series of 2D slices, as schematically illustrated in Figure 3.5.

3.3 Tomographic Reconstruction

When a series of projections of the object are available, the next step consists of reconstruction. Reconstruction and its mathematical formulation dates back 1917 (Radon). In this section only a basic understanding is presented.

Referring to Figure 3.6, in an arbitrary plane normal to the axis of rotation (z axis), the object is presented by a spatial function of X-ray absorption function, $f(x,y)$. Any set of X-rays passing through the object projects an absorption profile $L_z(x', \theta)$ on axis x'.

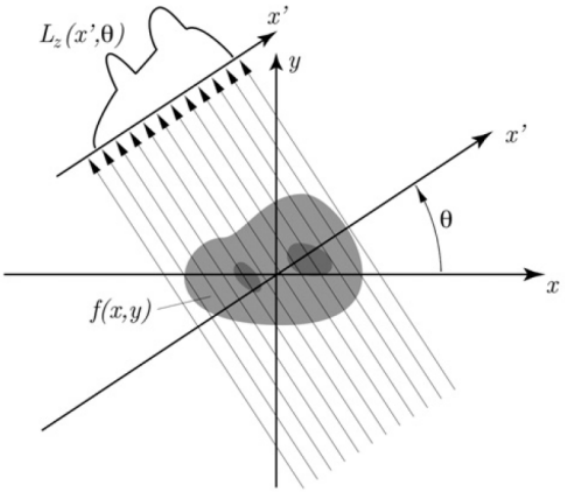

Figure 3. 6 - X-ray absorption model used for tomographic reconstruction [62].

A collection of these profiles for a particular slice at successive view angles, θ, is often represented as sinogram, formed by stacking all the projections of different views, so a single projection is represented by an horizontal line in the sinogram, Figure 3.7 and Figure 3.8 [62, 65].

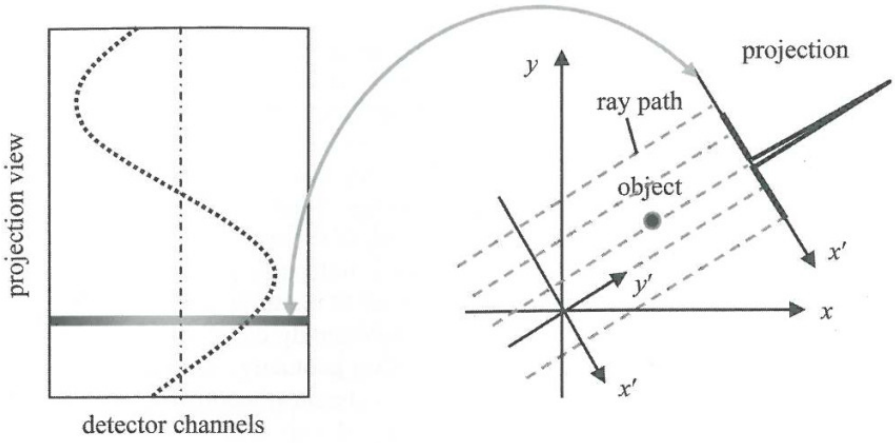

Figure 3. 7 - Mapping between the object space (right) and the sinogram space (left) for a single point [65].

If we plot a projection of a single point as a function of the projection angle, we obtained a sinusoidal curve, Figure 3.7. Since any objected may be approximated by a series of points, its projection will be overlapped sine or cosine in the sinogram space, Figure 3.8. A sinogram is a useful tool for analyzing projection data, and often is used to detect abnormalities in a CT data [65].

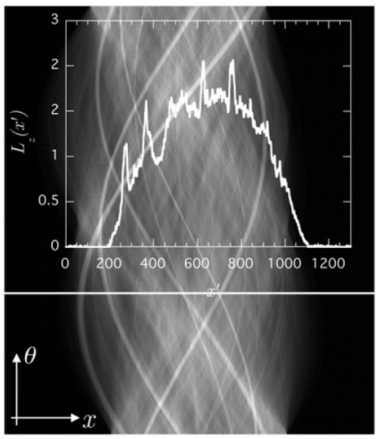

Figure 3. 8 - Sinogram of any complicated object is formed with overlapping sinusoidal curves (background) [62].

In tomographic reconstruction, the problem to solve is the inverse problem in which *f(x,y)* is determinate from a series of projection functions. While uniqueness can be shown for a continuous *f(x,y),* errors are introduced in the discrete process of acquisition and by the measurement processes. *Hsieh* [65] listed the main errors related to the projection acquisition process. The assumption that X-ray beam is monochromatic requires that all of the X-ray photons emitted have the same energy. The output spectrum of a laboratory X-ray tube is broad, resulting in a polychromatic source. As a consequence, the linear relationship between the measured projections and thickness does not exist. This problem is known as beam-hardening problem, which causes shading or streaking artifacts in reconstruction image. Another problem that affects the accuracy of the projection measurement, producing shading and streaking artifacts, is the presence of scattered radiation. A third source of measurement error may be the nonlinearity of the detector. A fourth source of error may come from the object itself, if there is any movement during the scanning, the projection obtained do not represent X-ray attenuation. These and many other sources of error that lead to CT image artifacts and inaccuracies. Computed tomographic reconstruction is not limited to the problem of image formation using ideal projections, but pre-processing and post-processing are important to reduce the aforementioned sources of errors [65].

In order to perform tomographic reconstruction, several types of different algorithms are developed, which included direct or iterative solutions. The theory that governs the Filtered Back Projection (FBP) method is known as Fourier slice theorem, known also as “central slice theorem”, which assumes that the Fourier transform of a parallel projection of an object

f(x,y) obtained at an angle θ equals a line in a 2D Fourier transform of *f(x,y)* taken at the same angle [65]. This concept is shown in Figure 3.9 for a projection at an angle of 0°.

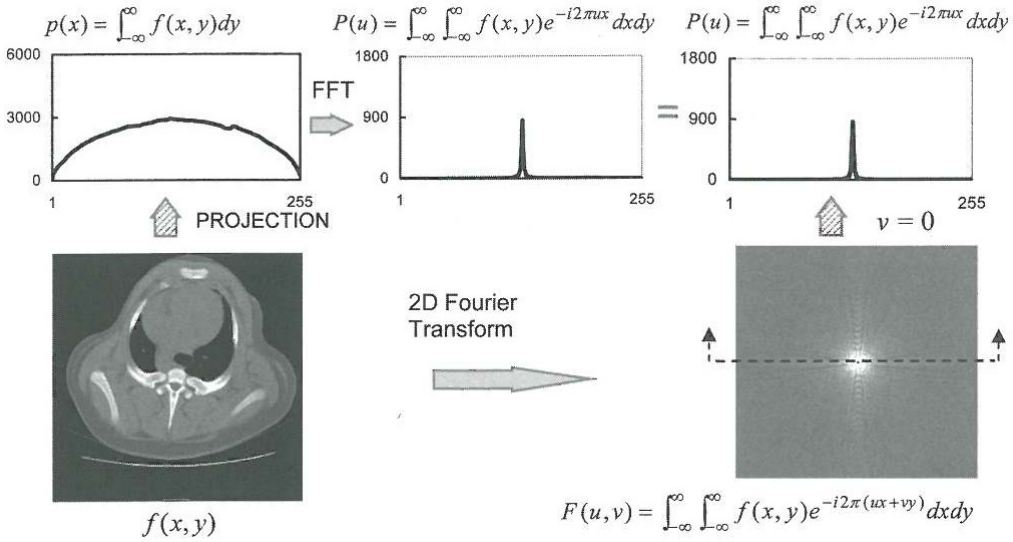

Figure 3. 9 - Fourier Slide theorem for a projection at an angle of 0° [65].

FBP is a direct method, based on the Fourier Slice Theorem, widely used for tomographic reconstruction. Back projection reverse the process of projection data to reconstruct an image, each projection is smeared back across the reconstructed image, as illustrated in Figure 3.10.

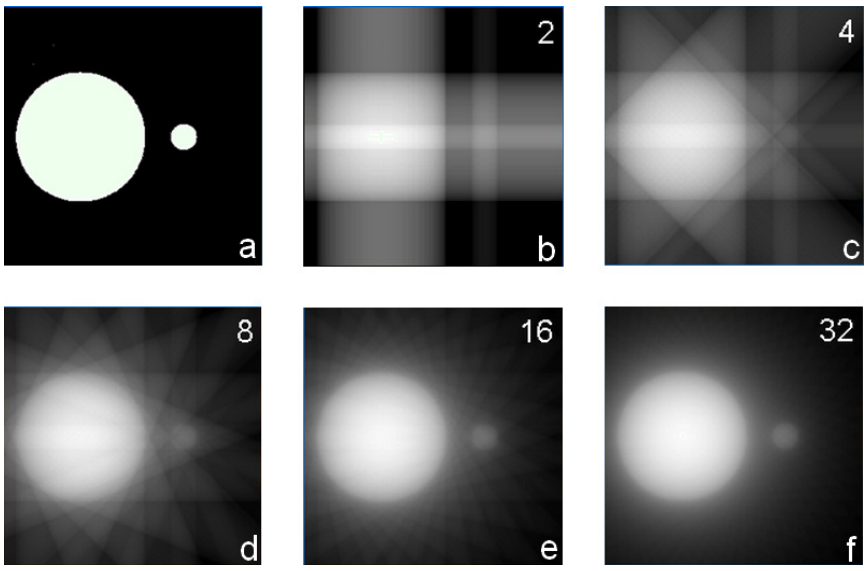

Figure 3. 10 - Back projection algorithm application for different number of projections. Original image (a) is reconstructed in for 2,4,8,16,32 number of projections respectively (b,c,d,e,f) [66].

Back projection produces blurred trans-axial images; therefore projection data needs to be filtered before reconstruction. i.e. a filtered back projection algorithm.

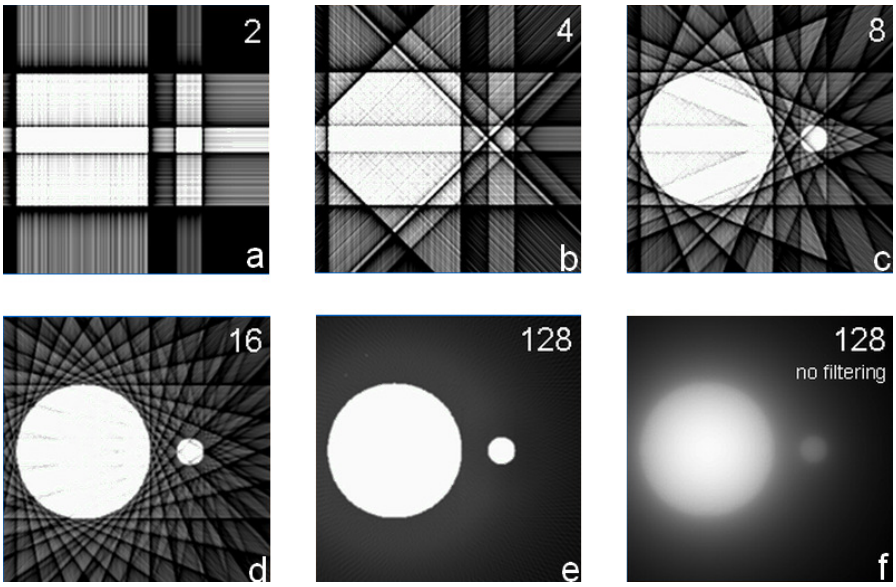

Figure 3. 11 - Filtered back projection algorithm application for different number of projections for 2,4,8,16,128 number of projections respectively (a,b,c,d,e) and comparison with back projection algorithm (f) [66].

Differences, in terms accuracy of the reconstructed image due to projection filtering may be observed, comparing Figure 3.10 and Figure 3.11.

Chapter 4 Material and Methods

4.1 Material

The material used in the present study was carbon/epoxy prepreg M21/T700 unidirectional (Hexcel) provided by Airbus. The nominal volume fraction of fibre is 70%. Toughening particles were dispersed in the resin, Figure 4.1.

Toughed high performance thermosetting matrixes are obtained with the addition of thermoplastic or rubber materials. Matrix mechanical properties result in a flexural modulus of 3.50 GPa and flexural yield strength of 147 MPa [67].

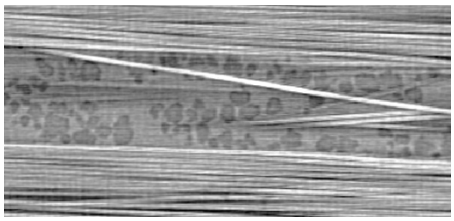

Figure 4. 1 - Toughening particle in the epoxy are visible, together with carbon-fibre (diameter 7 μm).

Laminates were produced with two different layups, $[90/0]_s$ and $[0/90]_s$; as indicated in Figure 4.2, 0° identifies the loading direction.

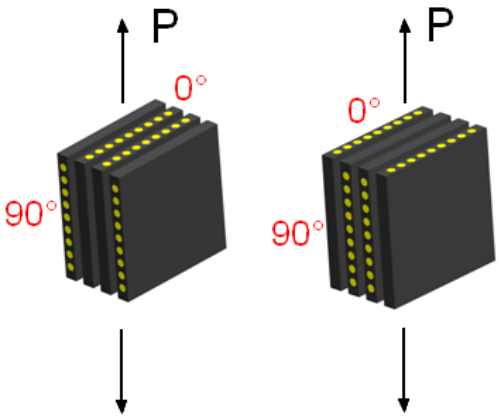

Figure 4. 2 - Stacking sequence used for preliminary fatigue tests, $[90/0]_s$ and $[0/90]_s$ respectively.

Sheets of 300x300x1 mm were initially manufactured using a process of consolidation [1], which consist of application of an initial pressure of 1 bar under vacuum, 7 bar in autoclave with an heat-up of 2°C/min until a dwell temperature of 180°C for 120 minutes, Figure 4.3. Finally, sheets are cooled to reach room temperature with a rate of 4°C/min.

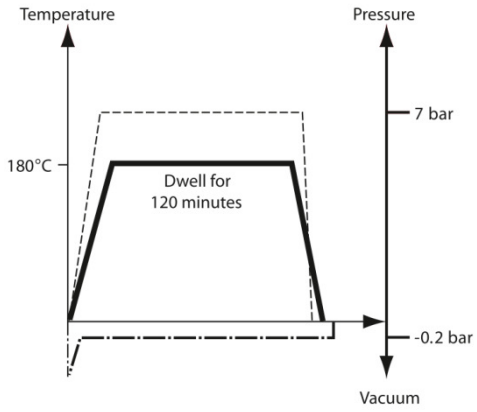

Figure 4. 3 - Schematic process of consolidation for composite with a thickness less than 15 mm [1].

Mechanical properties of M21/T700 for 70 % of fibre volume, are summarized in the Table 4. 1.

E_1 (GPa)	E_2 (GPa)	G_{12} (GPa)	ν_{12}	σ_{1ten} (MPa)	σ_{1comp} (MPa)	σ_{2ten} (MPa)	σ_{2comp} (MPa)	σ_{12} (MPa)	α_1 (K^{-1})	α_2 (K^{-1})
148	7.8	3.8	0.35	2200	-1280	75	-250	95	0	34 e^{-6}

Table 4. 1 - M21/T700GC mechanical properties [68].

Double-notched specimens were machined from plates using the abrasive waterjet technique. Traditional machining has several disadvantages particularly because the process involves the dissipation of heat into the workpiece. Jetting technologies overcome this limitation, operating in cold condition [69]. Using this technique specimens were realised with a width of 4 mm, thickness of 1 mm, length of 66 mm, and a notch radius of 1.5 mm, see Figure 4.4.

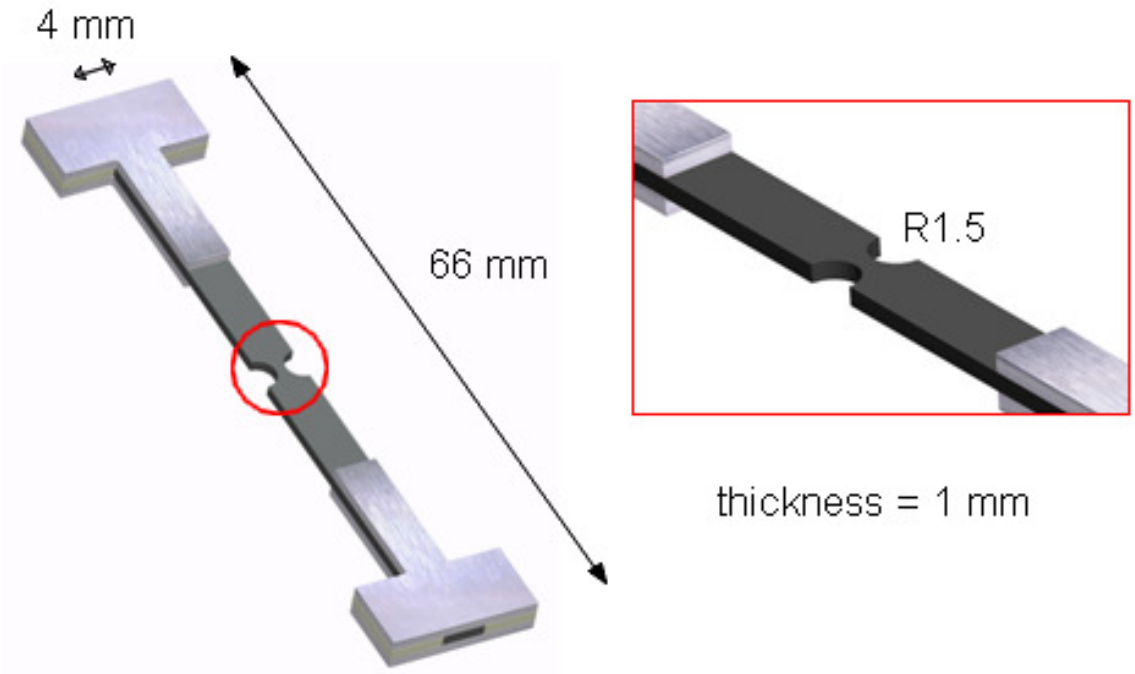

Figure 4. 4 - Schematic representation of specimen geometry and dimensions.

Aluminium tabs, produced by laser cutting, were bonded at the end of specimen using epoxy glue, in order to minimizing the effect of grips and increasing the area of the loading region, reducing local stress concentration. Using of tabs is regulated by the Standard Normative ASTM D 3479 [70].

Wright *et al*. in previous studies tested same samples to failure under quasi-static load, reporting an ultimate failure stress of 960 MPa across the notch section [71].

4.2 Instron ElectroPuls E1000

The system used to carry out fatigue loading was an electric dynamic machine: Instron ElectroPuls E1000. Essentially the main difference compared with traditional servo-hydraulic machines consists of having a single phase, linear motor, which gives the system a dynamic testing capability in the order of hundreds of Hz with low noise and without use of hydraulic oil.

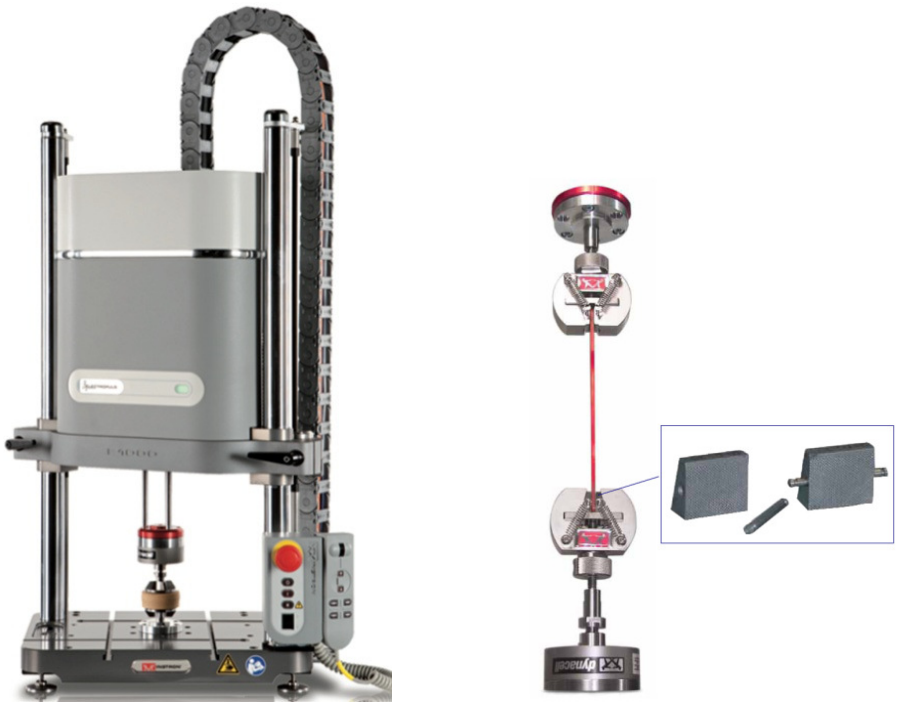

Figure 4. 5 - Instron ElectroPuls E1000, with the correspondent grips and faces jaws [72, 73].

This system is designed for dynamic and static testing and includes: advanced digital control electronics, DynacellTM load cell, Console software, and electrically crosshead lifts, illustrated in Figure 4.5. Regarding dynamic performance, load capability is ±1000 N with an accuracy of ±0.5%, and capable to operating at over 100 Hz. Actuator stroke is 60 mm [72]. Mechanical wedge action grips were used, which allow self-tightening, eliminating slippage Figure 4.5. The wedge action principle of the grips allows them to be tightened easily, by hand, onto the specimen without altering the vertical position of the faces in relation to the specimen. This design supports pre-selection of the exact point at which the specimen is gripped, choosing a proper gauge length, without compressive force applied, avoiding buckling phenomena. Jaw faces are serrated for optimum gripping performance and the serrations were designed to minimize damage in the specimen surfaces.

4.3 µ-VIS Centre: Metris HMX ST

The µ-VIS Centre, located at Highfield Campus in Southampton, is a dedicated centre for computed tomography and supports different fields, engineering sciences, biomedical sciences, environmental sciences, archaeological sciences and many others [74]. Range in

terms of specimen dimension is between 1-2 mm to 1.5 m, depends on the system, with the possibility to reach a resolution of 3 µm in standard operation. In this section, a brief description of the 225 kV Nikon/Metris HMX ST is provided (Figure 4.6), which was used to scan the present specimens.

Figure 4. 6 - HMX ST scanner at µ-VIS Centre [74], with a zoom of the internal configuration (right) where is possible to see the rotary stage and the X-ray source [75].

The object of interest is placed on a rotary stage between an X-ray source and detector. Moving the sample closer to the X-ray source increases the magnification of the resulting image. A high-precision microfocus source generates the X-ray radiation and transmits the X-ray through the sample. A digital flat panel detector captures a 2D image of the X-rays patterns that passed through the specimen. The HMX detector is a flat panel of 2048 x 2048 pixels, and sample dimensions and weights allowed ranging up to 300 mm and 50 kg respectively.

At the core of the XT H 225 inspection system is a 225kV microfocus X-ray source. Three configurations are allowed, depending on the flux intensity, in transmission, standard reflection and rotating target configurations [75]. Nikon also provided the software used for reconstruction, CT Pro and CT Agent, based on standard cone beam filtered back projection.

4.4 Swiss Light Source Synchrotron

The Paul Scherrer Institute performs research in three main areas: matter and materials, energy and environment, and human health. Among its facilities there is the Swiss Light

Source, a third generation synchrotron light source. With an energy of 2.4 GeV it provides photon beams of high brightness for research [76], see Figure 4.7.

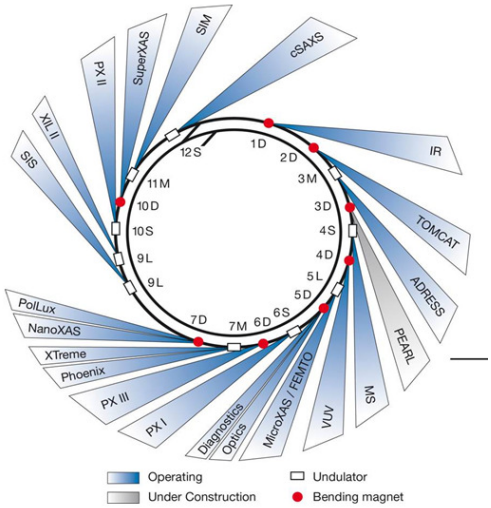

Figure 4. 7 - Beamlines schematization at Paul Scherrer Institute [76].

Each beamline is optimised for a specific technique. The beamline used to scan specimens related to this works, was TOMCAT (TOmographic Microscopy and Coherent rAdiology experimenTs), which received photons from a 2.9 T superbending magnet, this makes energies above 20keV easily accessible. TOMCAT provides monochromatic as well as white beam. Is possible to perform absorption as well as phase contrast imaging mode with a voxel resolution in the range of 0.36 – 14.8 microns. Acquisition times are in the order of few minutes, depending on resolution and energy [76].

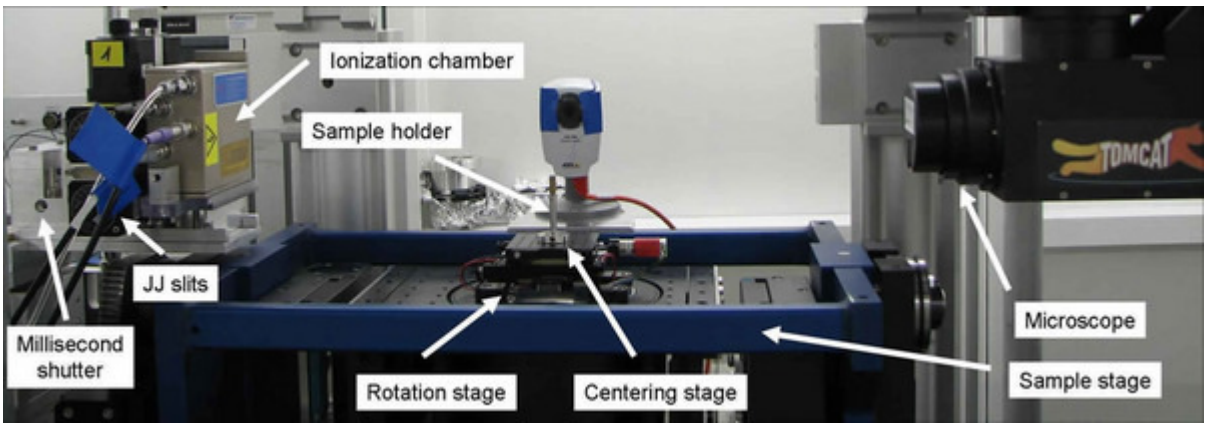

Figure 4. 8 – TOMCAT configuration for absorption and edge-enhanced tomography [76].

Figure 4.8 illustrates the main components of the standard configuration for absorption and edge-enhanced tomography. The TOMCAT endstation for microtomography allows translation along all three axes with a resolution better of 1 micron. The axis perpendicular to the beam direction has a reproducibility of 0.1 micron, this is important to avoid artefacts. A detailed image of the sample holder is shown in Figure 4.9.

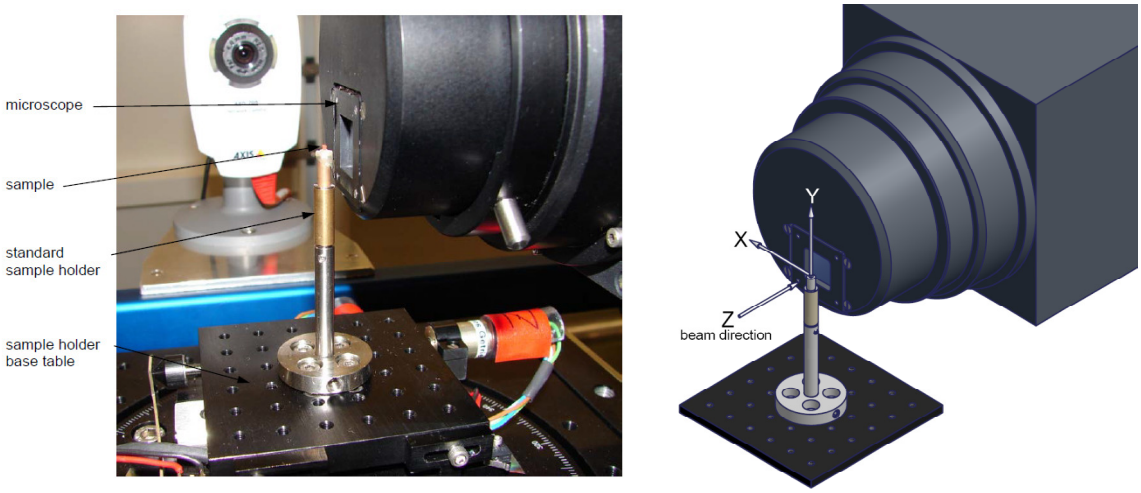

Figure 4. 9 - Sample holder and its schematisation [76].

4.5 X-ray Computed Tomography and Synchrotron Radiation Tomography

The main difference between X-ray computed tomography (X-CT) and synchrotron computed tomography (SRCT) is in the source radiation. In particular, for X-ray CT, photons are generated by a micro-focus X-ray tube, and this leads to a polychromatic divergent beam. Synchrotron CT uses synchrotron radiation to produce parallel, monochromatic and coherent beams, which represent the result of electron deflection within a high energy storage ring.
The difference in terms of source has important advantages for synchrotron radiation CT. One is represented by high spatial resolution (submicron). Another characteristic is the high temporal resolution, important when performing *in situ* experiments. High intensity of X-ray improves the signal to noise ratio in the images. Parallel and monochromatic beams avoid or reduce artifacts. High spatial coherence source, like synchrotron light, allows performing scans in phase contrast. This latter mode gives a better contrast compared to the pure

absorption. However, a disadvantage for synchrotron radiation CT consists in the limited specimen size and beamline availability.

4.6 Preliminary Fatigue Test

Specimens used for preliminary fatigue test were carbon/epoxy pre-preg M21/T700 with a layup of $[0/90]_s$ and geometrical properties as shown in Figure 4.4. The purpose of these tests were to assess damage generated inside the specimen when this is subjected to a cyclic load in order to make a calibration in terms of maximum load and number of cycles for subsequent experiments. This evaluation results important because the field of view which it is possible to achieve in a CT scans, depends of the resolution and the number of pixels of the detector used. The aim is to know roughly if the damage may fail inside or outside the field of view of the available equipment. As a consequence, is possible to plan the scans to perform. If the level of damage observed in a sample falls within the field of view, only one scan contains all damage, whilst, if damage is out of the field of view, more scans are needed to cover the damage.

Preliminary fatigue tests were characterised by ratio R=0.1, frequency of 10 Hz, number of cycles of 100, 1000 and 10000 respectively, and a maximum load of 108, 324, 540, 648 N. Parameters associated to these tests are reported in Appendix, Table A.1.

4.6.1 Setup of the fatigue tests

The first step consisted to regulate the mobile crosshead and actuator in an adequate position, in order to accommodate specimen in the test space, and at the same time to have the possibility to give to the actuator a sufficient stroke to transfer load. The next step was the specimen insertion in the grips. This procedure is particularly important because ensures the implementation of the test correctly, and specifications are given by normative [70]. In particular, the long axis of the gripped section must be aligned with the test direction, and specimen must be placed symmetrically in the grips space. Misalignments may produce unexpected failure modes and consequently invalidate the test. Because untabbed specimens were used, a folded strip of emery cloth between the specimen faces and the grip jaws (grit side toward specimen) was placed to avoid or reduce slip of the specimen in the grips. Each specimen was monitored in terms of slippage into the grips, recording the mean position of

the actuator, which should be the same during the test. After positioning specimen in the grips, grip jaws were tighten contemporaneously to avoid movements of the specimen, but not completely to avoid any bending effect on the notch zone. This was overcome using two thin steel layers with a larger surface than the notch zone, placed one from each side of the notch, locking the notch zone between them with a hand clamp. At this point jaw grips were tighten completely. Prior to carrying out fatigue experiments on the specimens, it was necessary to setup the equipment using the Instron Console® software, setting actuator limits, and calibrating of the system. Imposing limits position provides to have the control on the test and locks the machine in case something of unexpected happens and the actuator's position will be out of the imposed range. The last step consisted to transfer the system to load control, since tests were performed in load control, and carry out tuning using representative loads. Another Instron software, WaveMatrix, was used to create the test method. Essentially, fatigue tests were defined by creating a test sequence composed of three steps, as shown in Figure 4.10.

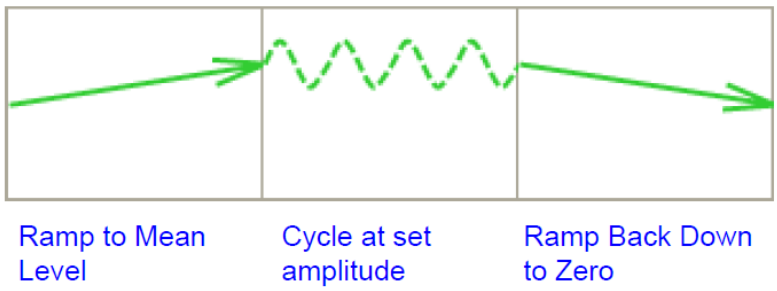

Figure 4. 10 - Steps to define a fatigue method.

The first sequence consisted in applying an initial quasi-static load starting from the current load after tightened the wedge grips, and reaching the mean value of the cyclic loading. The second step was the cyclic loading, this began from the end point of the previous step and finished at the same value, after a fixed number of cycles. Finally, a quasi-static ramp load allowed to unloaded the specimen.

Each test step is characterised by specific parameters, which are summarised briefly. The initial ramp presupposed a ramp rate, calculated assuming that the machine reached mean load in 30 seconds in the case of the lowest load considered. This leads to a loading rate of 1.6 N/s. Ramp rate was kept constant for all tests.

4.7 Preliminary Pre-Fatigue Scanned Specimens

After preliminary fatigue tests were performed, the associated samples were scanned at the μ-VIS Centre, using the 225 kV Nikon/Metris HMX ST. Specimens were stacked in blocks of three with the aim to gain time, including more specimens in one scan. X-ray energy was set to 50 kV, while current to 125 μA. Resulting voxel resolution was about 3.3 μm. Considering that dimensions of detector were 2000 x 2000 pixels, consequently the field of view obtained was 6.6 x 6.6 mm^2. The number of projections was 3141, and the exposure time of 2 second.

4.8 Fatigue Tests

On the basis of the results obtained by preliminary fatigue tests, fatigue tests were planned using the same material (carbon/epoxy prepreg M21/T700 unidirectional Hexcel), with the layup $[90/0]_s$, and the same double notched geometry. Fatigue tests were characterised by a ratio R=0.1, frequency of 10 Hz, number of cycles 10000, and two levels of load (300 N and 450 N), corresponding to approximately 30% and 50% of the tensile strength, respectively. For each load condition, three fatigue tests were performed.
Parameters associated to these tests are reported in Appendix, Table A.2. Setup of each single test was done using the same procedure and parameters mentioned for the preliminary fatigue tests.

4.9 Pre-Fatigue Scanned Specimens

All specimens cyclic loaded under low and high load (300 N and 450 N) were scanned at the μ-VIS Centre, by 225 kV Nikon/Metris HMX ST. Specimens were stacked in blocks of two, because in this case the global thickness was greater than the previous scans, due to the presence of tabs. Parameters for X-ray settings, and scan parameters, were maintained the same of the previous scans, presented in section 4.8. The resolution achieved was 6.2 μm, with a field of view of 12.4 x 12.4 mm^2.
Two specimens among various pre-fatigued specimens were chosen for SRCT imaging, one for each level of load. These were scanned at Swiss Light Source using synchrotron radiation. Beamline energy was set at 19 keV and ring current at 352.067 μA. The number of

projections collected through the rotation of 180° were 1500 and the exposure time for each radiograph was 150 ms. Resulting resolution obtained was 1.5 μm. Considering that the detector used had 2048 x 2048 pixels, the field of view resulting was of about 3 x 3 mm^2. For each specimen, scans were performed under two different conditions, unloaded and loaded respectively. In the unloaded condition a relatively little load was applied (38 N and 50 N for low and high load respectively) before the scan. Whereas, in the loaded condition, a load of 269 N and 409 N was applied respectively for low load and high load conditions, and after executing the scans. This condition allowed crack opening measurement. Two additional scans were performed for specimen tested at high load in order to include the crack tip, which fell out of the field of the first scan. In Appendix Table A.3, scans performed at Swiss Light Source were schematized. Using the same level of maximum load (302 and 454 N), two *in situ* scans were carried out at Swiss Light Source, applying a quasi-static load on a non-tested specimen. Beamline parameters were kept unvaried respect to the previous scans.

Chapter 5 Results and Discussion

5.1 Introduction

The chapter describes initial results obtained from tension-tension fatigue on carbon/epoxy composites in terms of qualitative and quantitative analysis. However, the results should be considered as initial results because their significance has not been demonstrated statistically. They represent a preliminary investigation of this phenomena, and providing a means to explore damage in composite materials using computed tomography techniques.

5.2 Preliminary Fatigue Test Results

As mentioned above, preliminary tension-tension fatigue tests were performed on $[0/90]_s$ carbon epoxy layup for various loading levels and for different number of cycles. After the reconstruction of the scanned volumes from the HMX device, visualization and post-processing analyses were performed using VG Studiomax 2.1. Image quality and resolution have proved suitable to distinguish qualitatively the different types of damage presented, except fibre breaks. VG Studiomax allowed visualization of 3D volumes, "slice" by "slice" in all directions, and also to measure features.

Experiments conducted in this phase, summarized in Appendix in Table A.1, have shown that for low levels of load, at about 10% of tensile failure σ_f, damage is not detected up to 10000 cycles. Intermediate loading, at roughly 30% σ_f, resulted in characteristic progressive damage growth in terms of onset and propagation, with an increasing number of cycles. Higher loads, showed the onset of all damage modes within the first few cycles and the propagation of these occurred with increasing numbers of cycles. This section focuses on two specific cases, corresponding to loads of 30% σ_f and 50% σ_f respectively.

A level of load equal to a 30% σ_f caused the onset and growth of transverse ply cracks at 100 cycles. Therefore, transverse ply cracks are the first type of damage detected. With increased numbers of cycles, 0° splits were formed in the notched zone, between plies with different orientations, and they grew along the fibre direction, as illustrated in Figure 5.1. Additional cycles affected the propagation of transverse ply cracks and splits that are already present, and also promoted the onset of other splits.

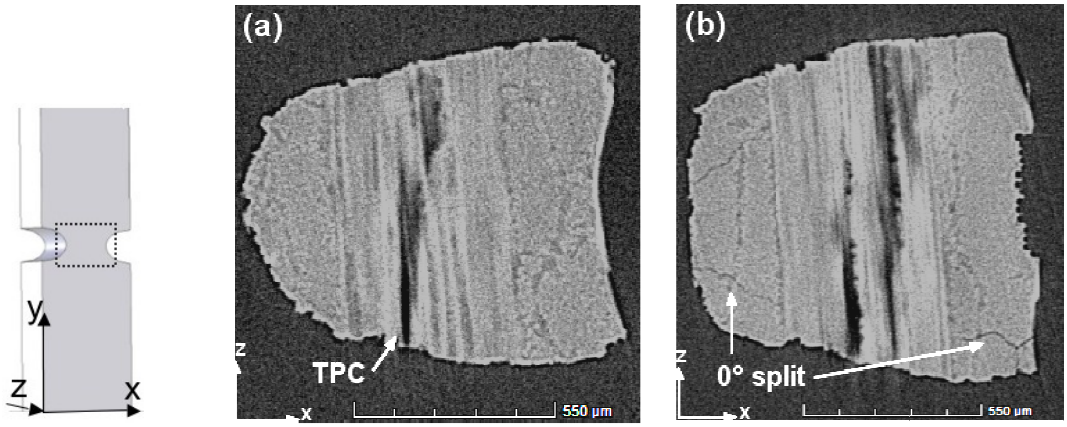

Figure 5. 1 - Comparison between damage detected at 100 cycles (a) and 10000 cycles (b) for a load of 30% σ_f.

At low levels of load, these tests showed that is possible to associate the onset and damage accumulation as dependent on the number of cycles.

Loading to 60% σ_f affected all damage initiation in few load cycles, including the presence of delamination at the ply interface. In fact, the case related to 100 cycles showed transverse ply cracks, splits and delamination, Figure 5.2.

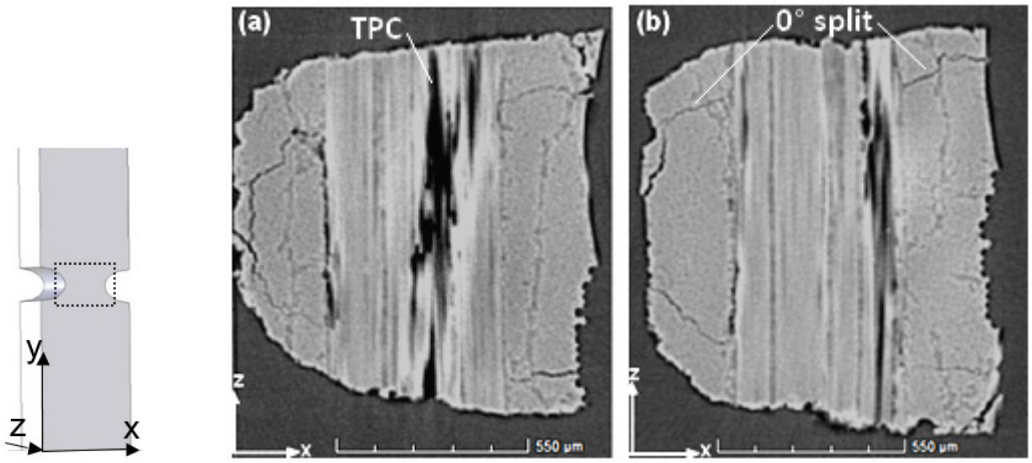

Figure 5. 2 - Comparison between damage detected at 100 cycles (a) and 10000 cycles (b) for a load 60% σ_f.

A quantification of damage propagation with cycle count is difficult to do in this situation, due to the quality of the images and associated noise and needs further investigation. In addition, splits extended out of the field of view, even at low numbers of cycles (Figure 5.3); therefore it was difficult to monitor their growth.

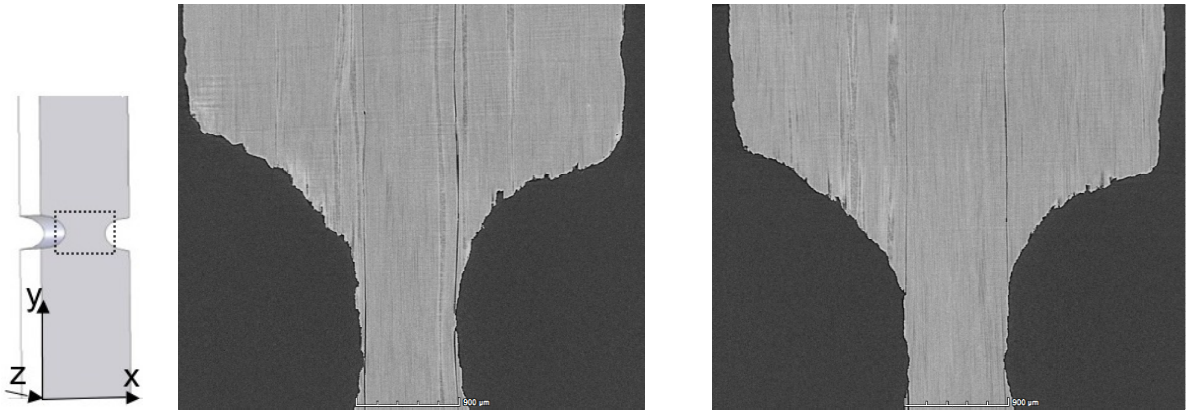

Figure 5. 3 - resulted outside of the field of view for a load of 60% σ_f., for both 100 cycles (a) and 10000 cycles (b).

Considering higher level of load, 70% σ_f, inspections revealed similar situation to the 60% σ_f, with an increase of damage extent, due to the higher loading. Results obtained from these preliminary fatigue tests supported the decision to perform subsequent tests for two level of load corresponding to: low load 300 N, and high load 450N respectively, and a number of 10000 cycles in order that damage fall in the field of view of CT scan.

5.3 Pre-Fatigue Specimens scanned using μ-VIS

In section 4.9 fatigue test parameters were detailed, also reported in the Table A.2, and the plan adopted for these *ex-situ* scans regarding pre-fatigue carbon/epoxy with a $[90/0]_s$ layup. Observations obtained from μ-VIS specimen's visualization had the aim to choose a specimen for each loading condition and define an appropriate window of view for the Swiss Light Source Scans. Considering the resolution of 1.5 μm and a detector with a number of pixels of 2048 by 2048, the window of view that it is possible to use is about 3x3 mm^2.
Therefore, due to the fact that specimen geometry is symmetric, it was chosen to scan half of each specimen, starting from the centre notch section. In particular, the region of interest began roughly 300 microns below the centre of notch and extended up to the limit of the detector dimension.

5.4 Segmentation Technique

Segmentation is a process which consists of segmenting image volumes by regions, and in this specific case allows a 3D representation of damage to be obtained. The principal method used in VG Studiomax to achieve segmentation is the region-growing algorithm. Region growing is an image processing technique that segments all voxels connected to a seed point and that are within a tolerance, defined by the user for the voxel (greyscale) values. Essentially, the procedure followed to segment a crack schematically in Figure 5.4.

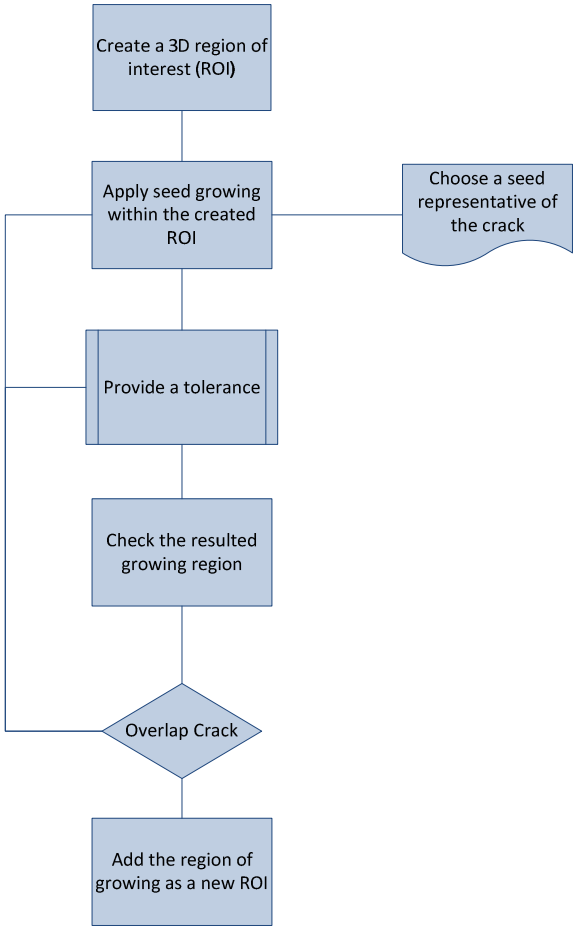

Figure 5. 4 - Flow chart of the iterative segmentation process.

The process is iterative until all pixels that describe the crack are included in a new region of interest (ROI), which represents the segmented crack. At this point it is also possible to extract the segmented damage as a new volume in order to visualise this in 3D, fully rendered, and choosing a specific colour it is possible to differentiate damage from the neighbouring materials. The principles of seed growing algorithm are quite simple, however

the results obtained depend on image quality and will also vary by user, who have to select seed growing and monitoring the process during the iterations. The main disadvantage is that this results in a time consuming process. In addition, the segmentation has been complicated by specific issues, which required additional time. These latter are related to the presence of discontinuous cracks. When the crack is discontinuous, the algorithm is not able to capture the entire crack with a limited number of seeds growing, because the tolerance imposed by user lock the algorithm propagation.

However, is not possible to give a bigger tolerance, because this would result in having an overestimated segmentation for the crack. The only solution in this case was to add many small regions of growing and merge these. Consequently, time spent to segment discontinuous cracks is increased. The other problem connected with the segmentation process is linked to the greyscale, which characterises the crack. If the crack opening is relatively small, its greyscale is roughly uniform, while for greater opening cracks, their typical greyscale cover a wider range, as illustrated in Figure 5.5.

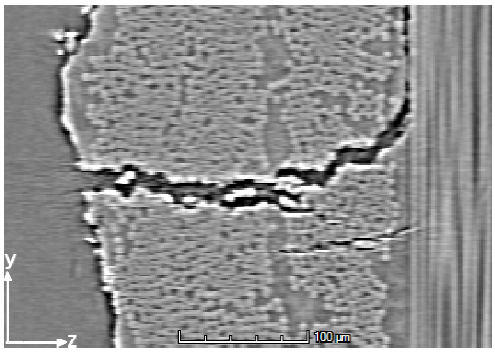

Figure 5. 5 - Typical greyscale range of a transverse ply crack with a high crack opening displacement.

The direct consequence consists in the impossibility to include the crack only selecting dark pixels as seeds growing, because inside the crack are present also other values of greyscale. In the same time, choosing as seed points all values of greyscale present in the crack lead to incorporate all the area around the crack. In this specific situation segmentation began a manually process, with consequently increase in time consuming.

Segmentation is an important tool to assess damage, especially when damage is three dimensional such as in composites. These limitations highlight the necessity to improve segmentation techniques with the aim to have greater control of the process and implement automation to reduce operation time.

5.5 Micromechanic Characterisation

5.5.1 Transverse ply cracking

Several transverse ply cracks were observed for both load conditions. However, it was not possible to capture their evolution in terms of nucleation and propagation at this preliminary stage. To assess their evolution, tests at different number of cycles are required: this will be investigated in future work.

Transverse ply cracks assumed various shapes and configurations within the same specimen.

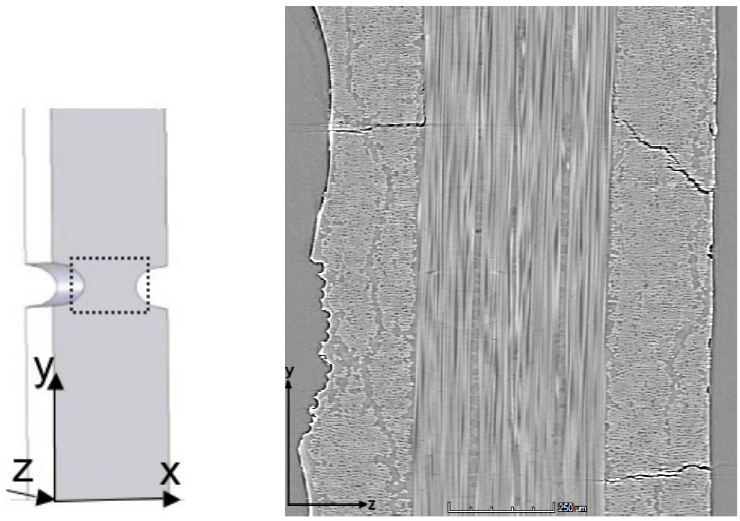

Figure 5. 6 - Transverse ply cracks shapes within the y-z plane.

Figure 5.6 shows three transverse ply cracks in the same specimen that have different propagation extents and consequently different shapes along the width of the ply. Bright fringe around the cracks results from phase contrast. Mechanisms that drive the transverse ply cracks propagation along a path or another, are unknown and need further investigation. Observations from these initial analyses illustrated that transverse ply crack shapes are dependent to the microstructure.

A single transverse ply crack in y-z plane was considered, Figure 5.7; plotting its shape in the x-y direction. It appears clear that the propagation through the 90° ply width depends on the microstructure.

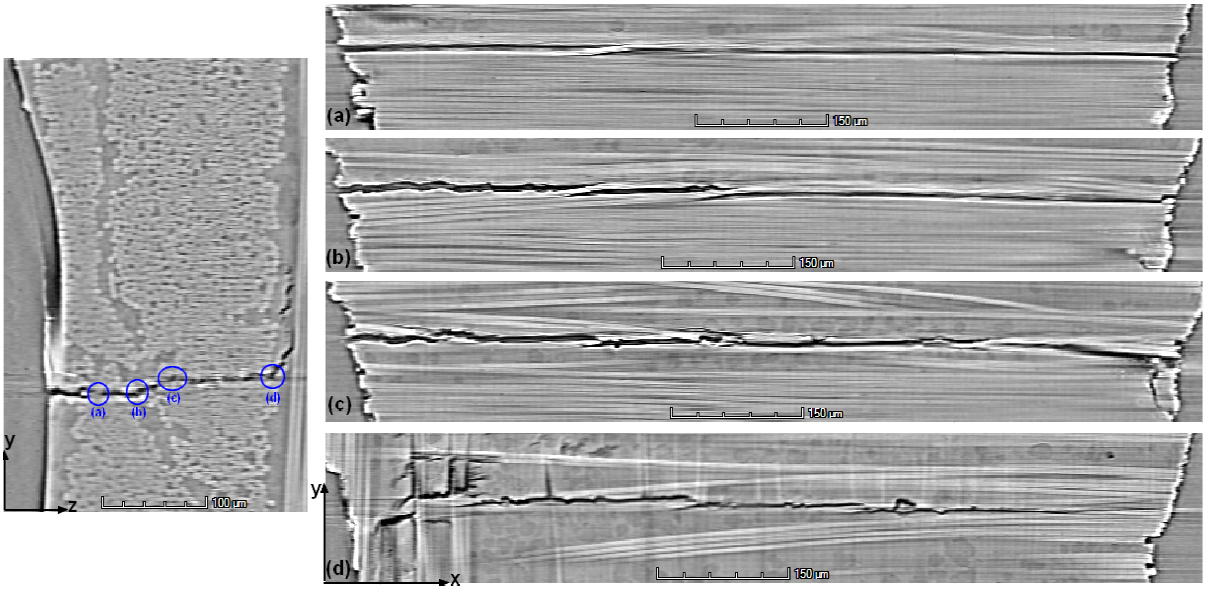

Figure 5. 7 - Transverse ply crack along the y-z plane and its propagation through the 90° ply width for a load of 30% σ_f.

In particular, Figure 5.7 (a), illustrates the propagation along a fibre rich zone, which appears straight and smooth with possible fibre bridging across the crack flanks. Figure 5.7 (b) shows the propagation along a resin rich zone that is serrated, while Figure 5.7 (c) results in a combination of resin rich region and some misaligned fibre across the crack. Loads were not supported by this bundle of misaligned fibre and consequently these broke. The last section Figure 5.7 (d) is in correspondence to the interface: interacting mechanisms between transverse ply crack and delamination are seen.

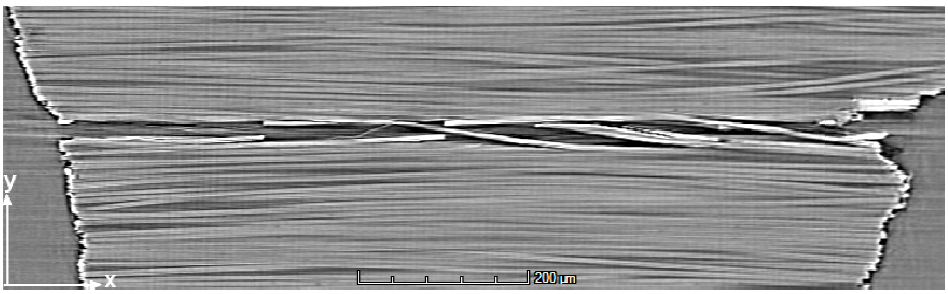

Figure 5. 8 – Typical fibre bridging and fibre breaks across a transverse ply crack.

At higher loads (50% σ_f), a greater crack opening displacement is seen. When the transverse ply crack propagates through a fibre rich region, some misaligned fibres bear the stress and act as a ligament across the crack (fibre bridging), while others reach failure, see Figure 5.8.

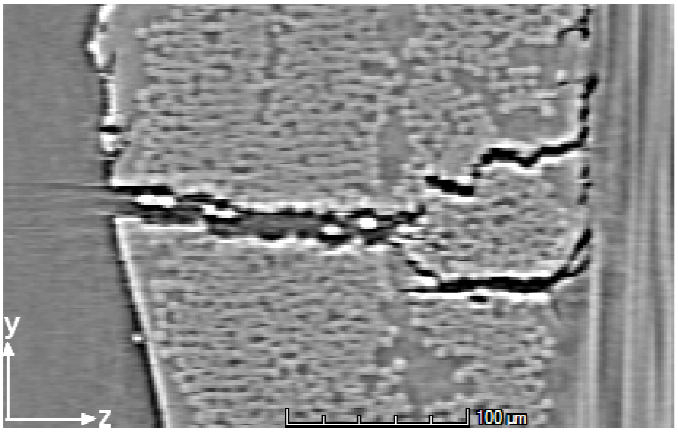

Figure 5. 9 - Bifurcate transverse ply crack.

Transverse ply cracks are again not always flat along the 90° ply width, but they also may assume discontinuous configurations, as illustrated in Figure 5.9, where the crack appears to bifurcate.

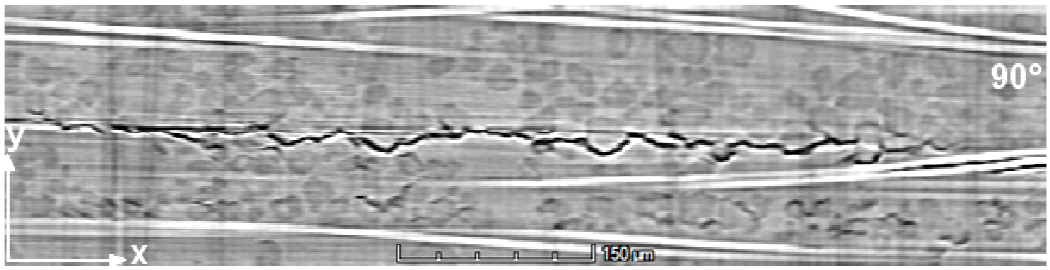

Figure 5. 10 - Transverse ply crack interacting with toughening particles.

As noted previously interfaces are essentially composed of resin rich region in this system, and consequently contain a high volume of toughening particles. Transverse ply cracks evolve in a discontinuous manner from toughening particles, which seem apparently to debond, creating a preferential path, as shown in Figure 5.10.

5.5.2 Splits

Splits has already mentioned are located in the 0° ply and develop in the loading direction. Sequence of their nucleation considering both sides and their propagation was not detected in this phase. Figure 5.11 confirms that split growth along the 0° plies depends of microstructure. Figure 5.11 (a) represents a section close to the interface, where the 0° split

interacts with delamination, creating a link between intralaminar and Interlaminar damage. Figure 5.11 (b) shows the split propagation in a resin rich region; the split has a non uniform, discontinuous and serrated configuration. Figure 5.11 (c) represents the split development in a fibre packed region, which is straight and smooth.

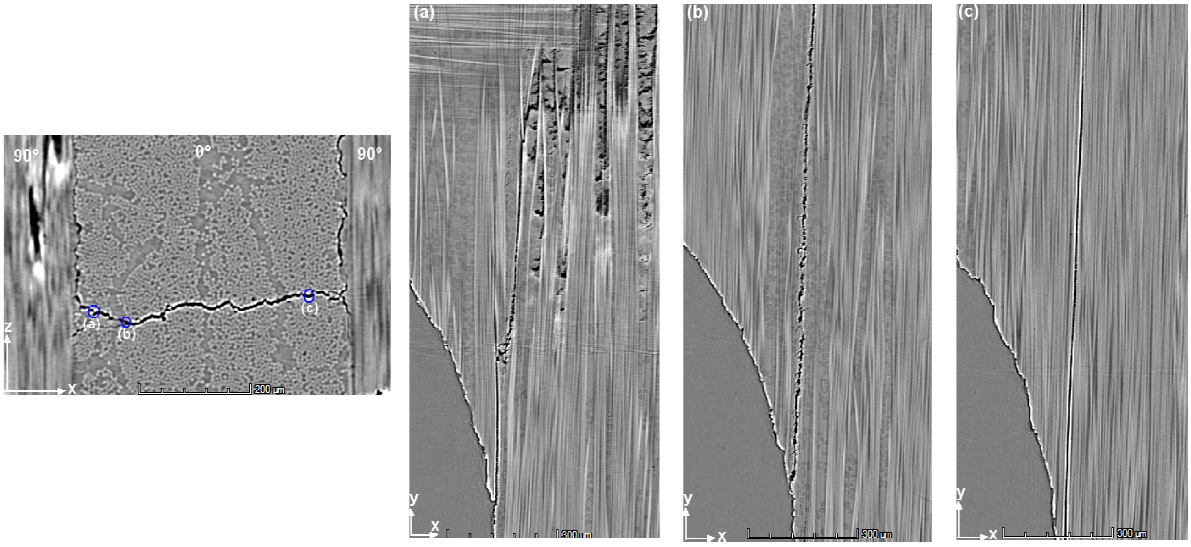

Figure 5. 11 - Different configuration for splits propagation along 0° ply width.

This analysis underlined the difference between splits growing between resin rich regions and fibre rich regions, which was further investigated. In particular split damage in the resin rich region, as illustrated in Figure 5.12, is in the form of small hackles and echelon cracks.

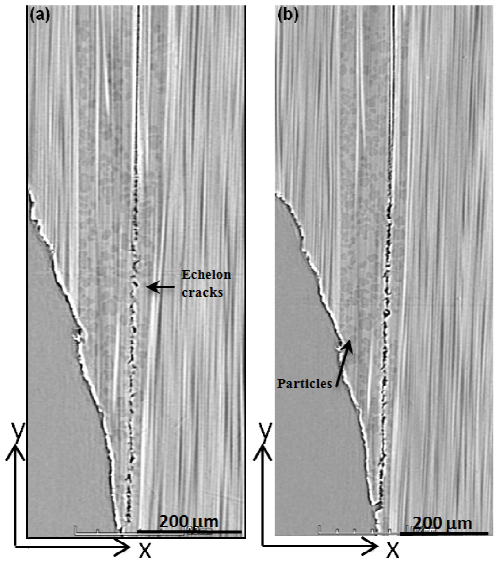

Figure 5. 12 - Echelon cracks along the split in the unloading condition (a) and loading condition (b).

Material between the echelon cracks provides bridging across the split. Toughening particles, which interact within the split in the resin rich region are also observed. Fibre misalignment and fibre breaks were observed along the splits. In some circumstances fibre misalignment are the cause of fibre breaks, as illustrated in Figure 5.13.

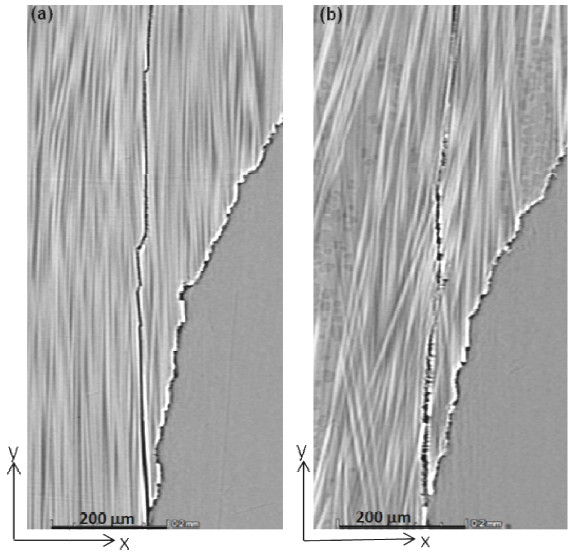

Figure 5. 13 - Fibre breaks along a 0° split (a) and fibre misalignment associated with fibre breaks (b).

When the split interacts with a broken fibre, the split front propagation jumps across the fibre, deflecting its trajectory, but always maintaining an overall direction parallel to the loading direction; in other hands, the split follows the fibre direction.

5.5.3 Delamination

Delamination extended at the interfaces between the plies with different orientation, Figure 5.14. Behaviour of this damage is complex to analyse, due to the fact that usually delamination appears when transverse ply cracks and splits are already formed and interacts with them.

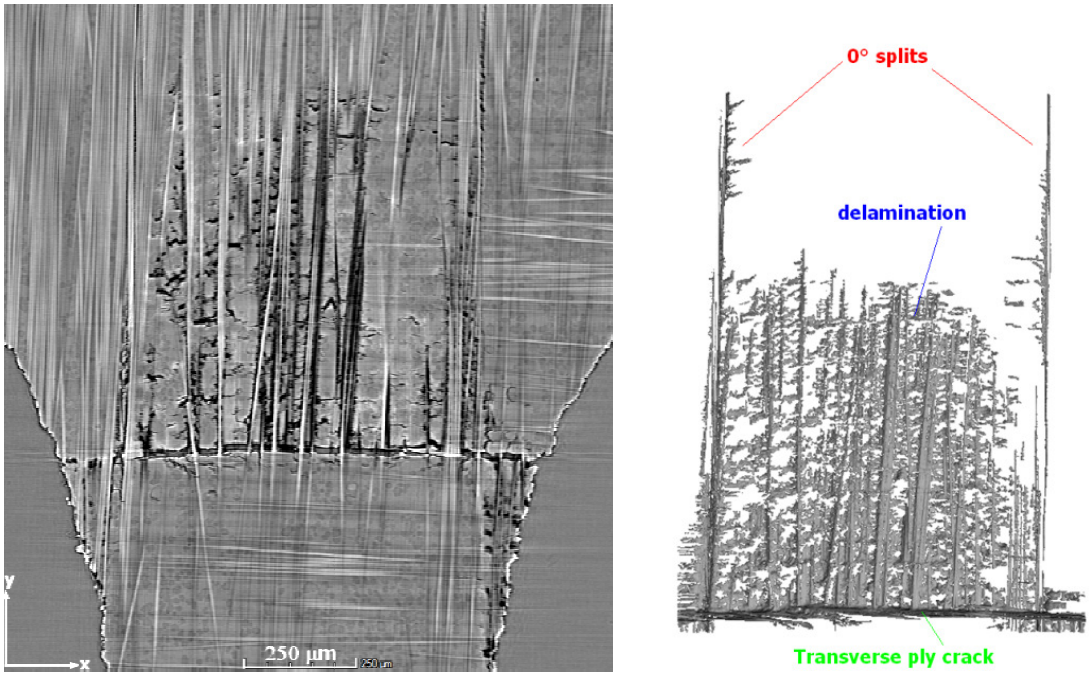

Figure 5. 14 - Delamination with the correspondent segmentation.

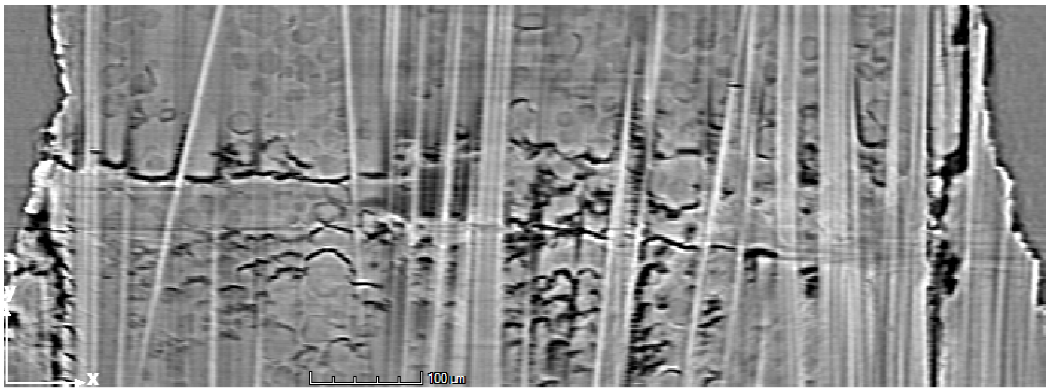

Figure 5. 15 - Toughening particles interacting with delamination.

2D slices showed a convergence between these different types of damage, for which delamination links transverse ply crack present in the 90° ply with the splits in the 0° ply. Figure 5.14 also illustrates the different in propagation along fibre and resin rich zone. In fibre rich regions, damage appears as “streaks” that follow the fibre direction, while in the resin rich region is presented in the form of many cracks, Figure 5.15.

5.6 Pre-Fatigue Specimens scanned at the Swiss Light Source

5.6.1 Low Loading Specimens

The 3D fully rendered damage segmentation corresponding to 30% σ_f load for 10000 cycles shows intralaminar damage present within the specimen in loaded and unloaded condition, Figure 5.16 (a) and (b). The notch surfaces have a rough appearance due to the water jet process used to cut the specimens, however in previous work, samples were scanned prior to loading and it was proved that cutting process did not cause damage that grew in subsequent loading [68].

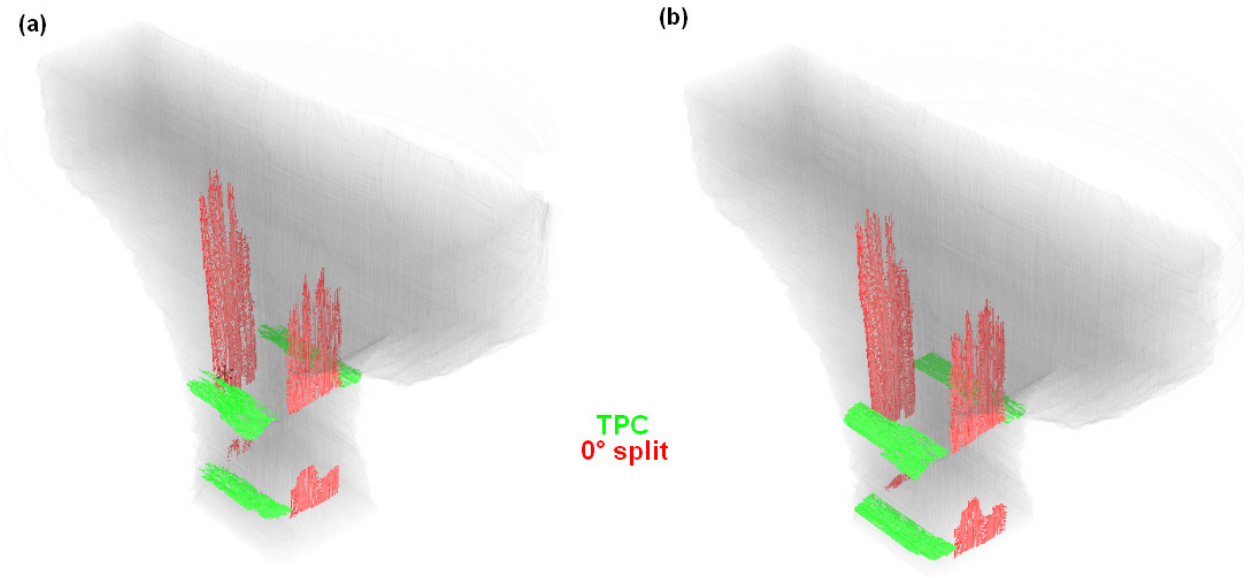

Figure 5. 16 - Damage for a load of 30% σ_f in unloaded (a) and loaded (b) condition respectively.

Damage segmentation illustrates the presence of transverse ply cracks in the 90° plies, and splits in the 0° plies. Transverse ply cracks appear completely developed across the width of the 90° ply and are located in the notch zone, close to the 0° split initiation region. Experiments performed did not describe from which side of the notch the transverse ply cracks initiated and how they developed along the ply width, because at this number of cycles, transverse ply cracks are completely developed across the ply width. Future work will be performed at different numbers of cycles with a view to assessing transverse ply crack initiation and propagation. Splits initiated at the notch zone and develop, above and below

this from both sides, within the 0° ply. They propagate in the loading direction, with a local rate that depends on the microstructure. Assuming the crack front is not uniform, but is characterised by retarded zones, typically resin rich regions, and tips, corresponding to fibre packed zone, Figure 5.17.

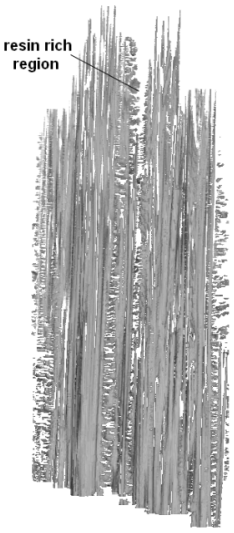

Figure 5. 17 – Typical segmentation of a 0° split.

Based on 3D segmentation, no significant differences seem to distinguish between splits in the loaded and unloaded conditions, and they seem to have similar shape and dimension. However, this is just a qualitative observation, and subsequent analyses will be conducted to investigate and characterise quantitatively splits in unloaded and loaded condition.

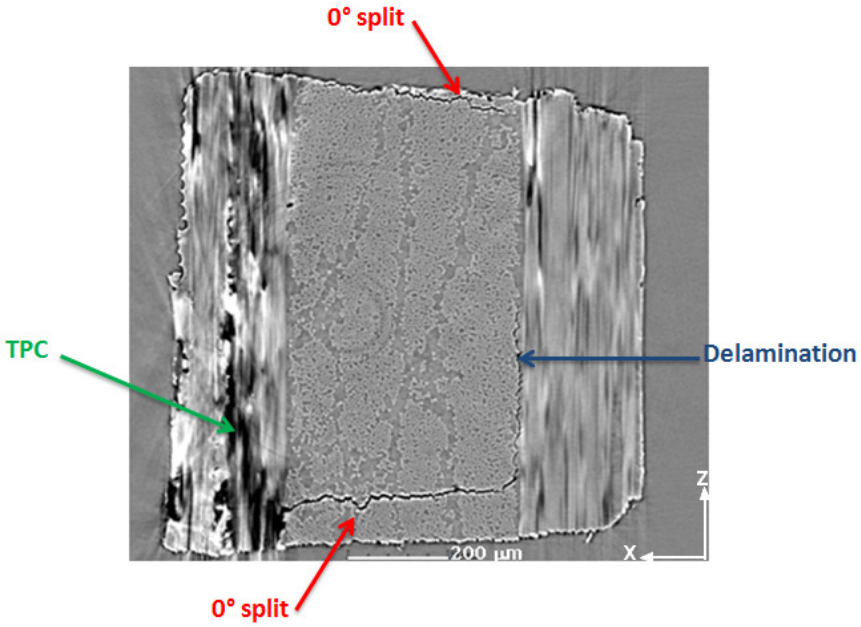

Figure 5. 18 - Schematisation of damage in the $[90/0]_s$ specimen, top view (x-z).

The 3D damage visualisation has revealed that both transverse ply cracks and 0° splits are not planar and propagate by following the ply direction in which they were formed. Interlaminar damage was observed also for the low level loading, in the form of delamination that is located at the 90/0 and 0/90 interfaces, respectively, as illustrated in the Figure 5.18. These delaminations have a rough fracture plans containing micro-cracks that originated at the interface, see Figure 5.19.

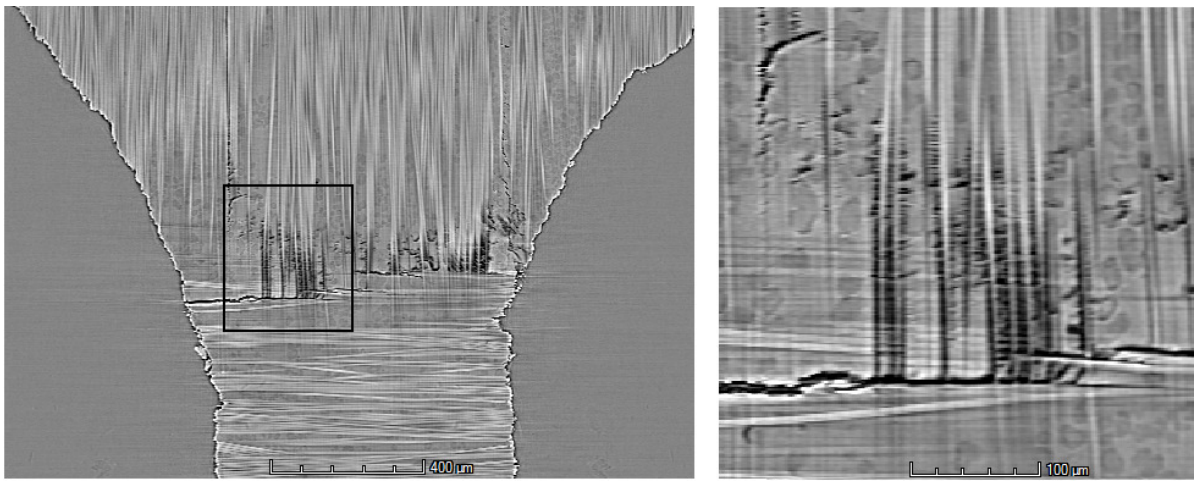

Figure 5. 19 - Delamination zone at the interface.

No relevant differences were noted between the 90/0 and 0/90 interfaces.

5.6.2 High Loading Specimens

Essentially fatigue high load exhibited a similar behaviour of the low load, however high loads involves in greater damage extent, Figure 5.20.

Transverse ply cracks in this case did not all completely propagated through the 90° ply: two of them initiated on the left hand notch and did not reach the other side. In addition, comparing Figure 5.16 and Figure 5.20 it is possible to observe an increase in number of transverse ply cracks for higher load.

Splits, located in the 0° ply, are more developed compared with the low loads, and extend out of the field of view. Segmentation in Figure 5.20 shows only the initial part of the splits, where damage is more uniform.

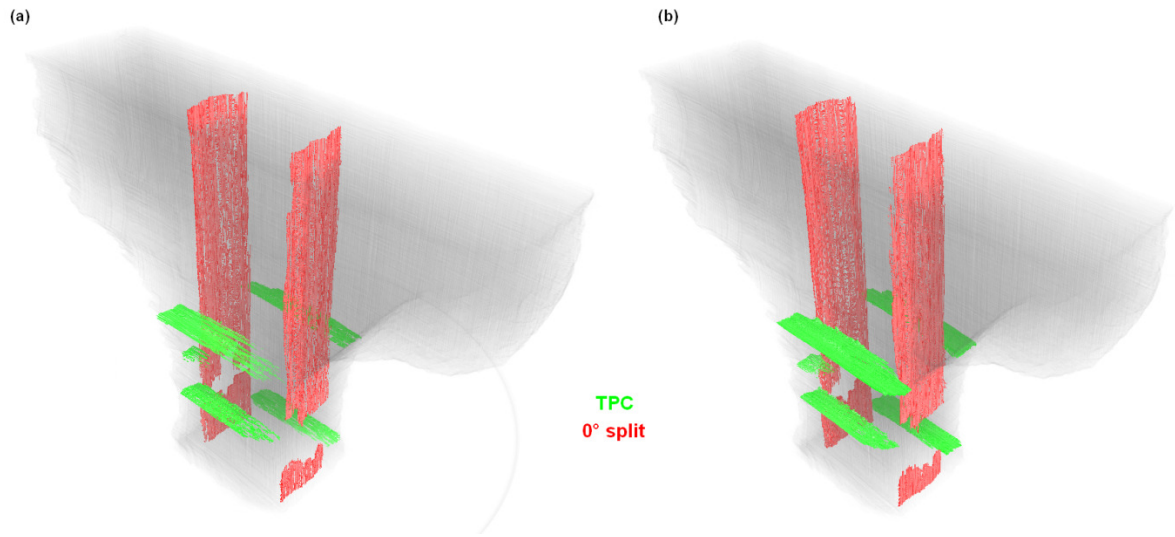

Figure 5. 20 - Damage for a load of 50% σ_f in unloaded (a) and loaded (b) condition respectively.

Additional scans were carried on, choosing a window of view that it could take the tips of the splits. Segmentation of this final part of splits has confirmed a similar shape of that found for low loading condition, Figure 5.21.

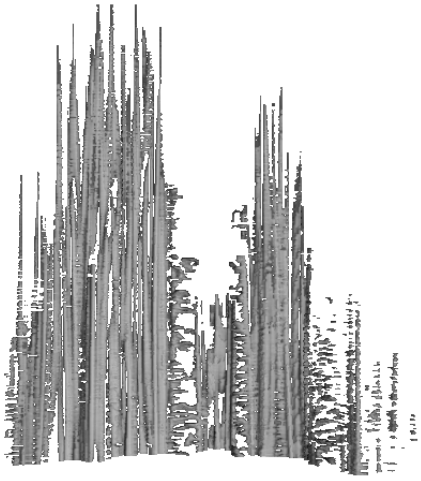

Figure 5. 21 - Tip split of a 0° ply for high load condition, 50% σ_f.

Delamination, present at the ply interfaces, is more developed than the low loading case. Figure 5.22 illustrates the segmentation of delamination at a 90/0 interface.

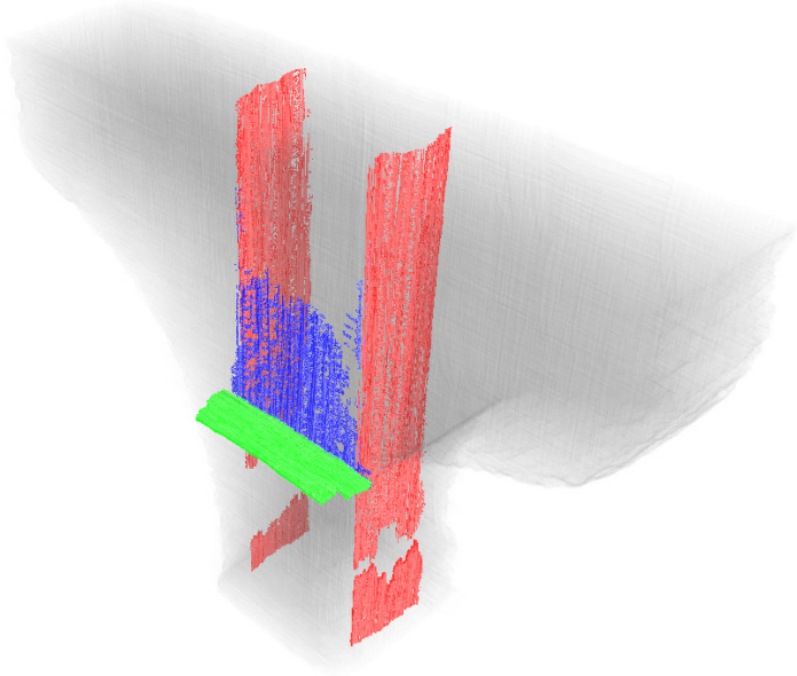

Figure 5. 22 - Segmentation of delamination at a 90/0 interface for a load of 50% σ_f.

The mutual position between transverse ply cracks, splits and delamination may imply interactive mechanisms that will be object of future investigation.

5.7 Crack Shear Displacement

The crack shear displacement associated with the 0° splits can be assessed tracking the movement of some features in terms of displacement between the unloaded and loaded condition. As already mentioned for crack opening displacements, crack shear displacements present in the unloading condition represents the contribution due to the residual stresses, while that measured in the loading condition is due to both residual stress and mechanical loading, and consequently the difference between values obtained for the unloaded and loaded condition is the amount due to only the applied mechanical loading.

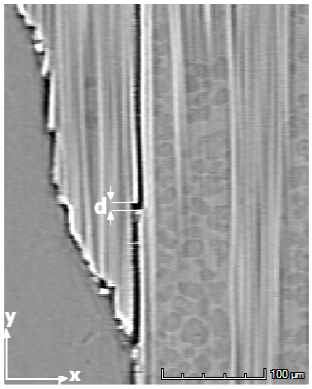

Figure 5. 23 - Fibre broken displacement using for determining the crack shear displacement.

In this context, broken fibres were taken as markers, and measuring manually, the displacement between the two sections of fibre, crack shear displacement was obtained, Figure 5.23. The total crack shear displacement obtained as a function of the distance from the centre of the notch, for low and high fatigue loading conditions, were shown in Figure 5.24 (a) and (b) respectively.

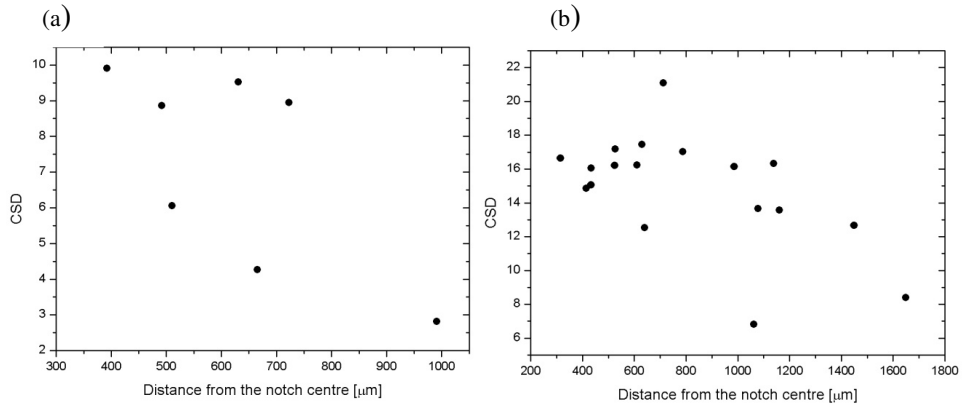

Figure 5. 24 - Crack shear displacement with the distance from the centre of the notch, for a load of 30 % σ_f (a) and 50 % σ_f (b).

Figure 5.24 illustrates that crack shear displacement depends on the position along the split, and in particular this decreases towards the crack tip. Although the data is quite scattered, the global trend appears to show a decrease with the distance from the centre of the notch. Further studies are required to investigate the single contribution due to residual stress and mechanical loading and investigate their influence on the total crack shear displacement varying the number of cycles and the loading level.

5.8 Comparison between Quasi-static and Fatigue Loading

A qualitative comparison between quasi-static tensile loading and cyclic loading can be achieved by inspecting the damage present in the static loading, Figure 5.25, with that associated to cyclic loading, Figure 5.16 and Figure 5.20. The first thing that appears evident is that damage in fatigue is greater in extent. However, damage location and shapes are quite similar between the two loading conditions. An important difference is the absence of delamination for quasi-static loading in correspondence at these load levels.

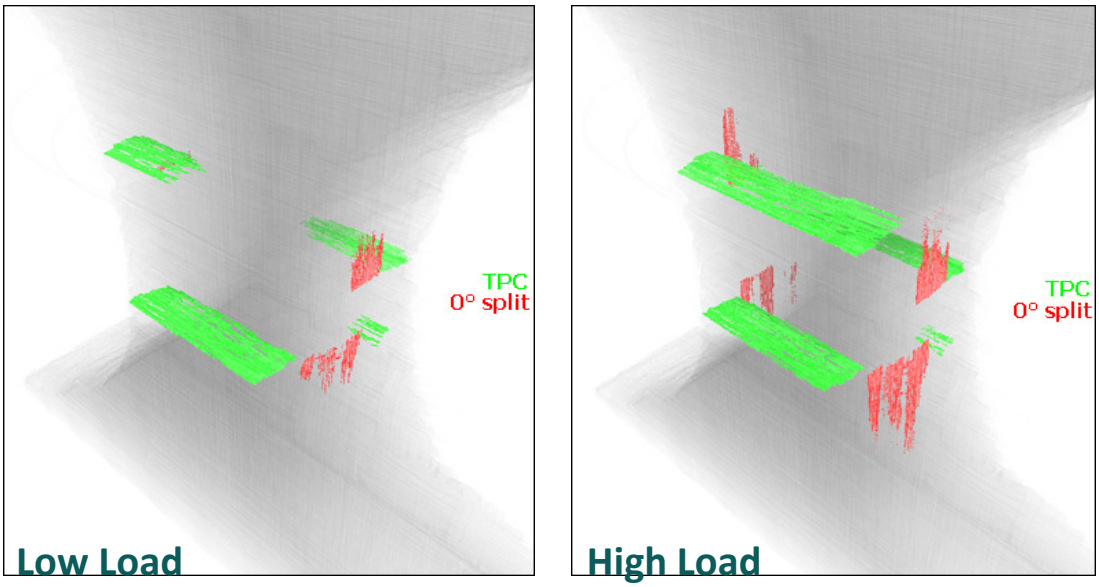

Figure 5. 25 - Damage for quasi-static tensile loading, for a load of 30% σ_f and 50% σ_f.

Damage segmentation for the two different loads, using the same specimens, allows to observe the damage development (Figure 5.25). Transverse ply cracks initiated on one notch side and propagated across the 90° ply width to reach the other side. Splits, like in fatigue loading, nucleated in the notch zone and propagate along 0° ply in the loading direction.
Micromechanistic comparison between quasi-static and fatigue loading showed a similar behaviour in terms of damage/microstructure interacting, Figure 5.26 and Figure 5.27. Micromechanics analysis for quasi-static loading was conducted in previous studies [21, 68], and using in this contest to make a comparison.

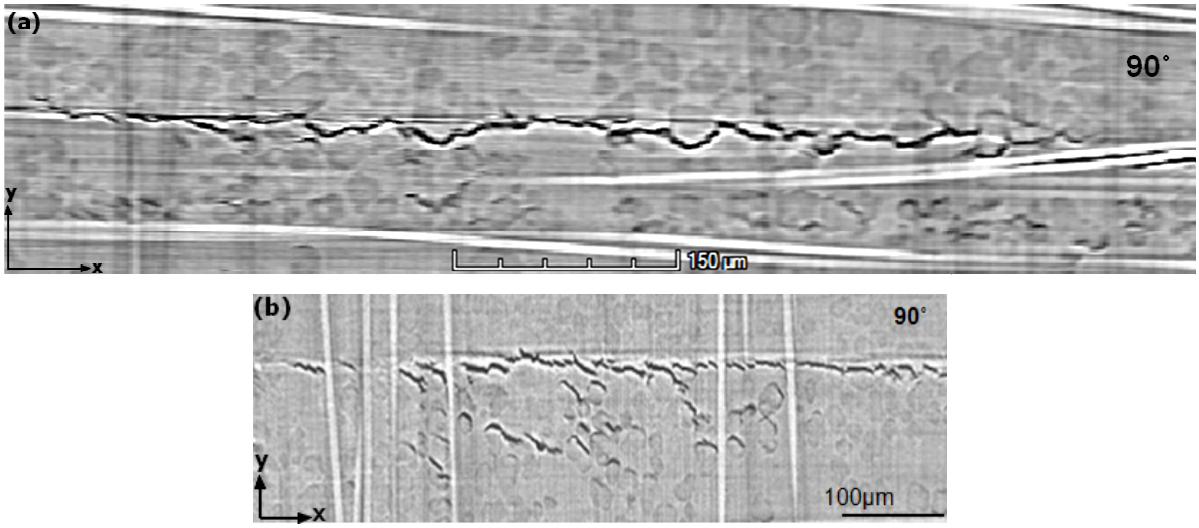

Figure 5. 26 - Transverse ply crack for fatigue (a) and for quasi-static (b) loading.

Figure 5.26 reported the 2D slice of a transverse ply crack close to the interface for fatigue (a) and for the quasi-static loading (b). Damage associated to quasi-static loading is discontinuous: resin ligaments across the transverse ply crack have a function of bridging. Whereas, fatigue damage appears more continuous and consequently with less ligaments.

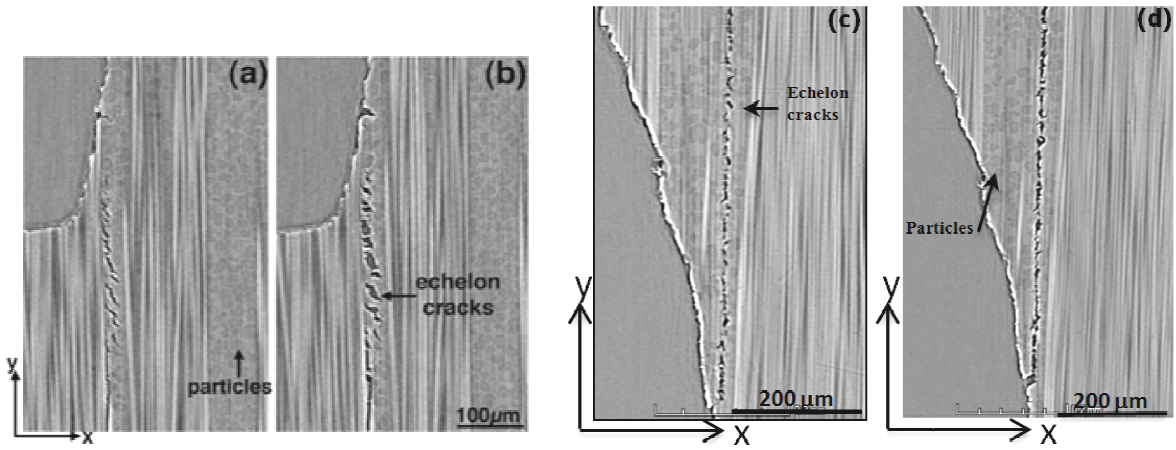

Figure 5. 27 - Split growth in resin rich region for quasi-static loading [21], unloaded (a) and loaded (b), and for fatigue, unloaded (c) and loaded (d).

Figure 5.27 shows a direct comparison of split propagation in rich resin region and fibre rich regions between quasi-static, Figure 5.27 (a) and (b), and for fatigue (c) and (d) in unloaded and loaded condition. Damage behaviour is similar, but in the quasi-static loading more diffuse bridging is present between echelon cracks, whereas in fatigue loading damage shows

less material bridging. This is more evident in the loading condition, Figure 5.27 (b) and (d), where for quasi-static load (Figure 5.27 b) damage observed appear in form of single microcracks with an orientation of 45° respect to the fibre direction; while fatigue damage is serrated and more continuous (Figure 5.27 d).

Conclusions

The initial part of this project had the objective to assess damage due to tension-tension fatigue loading using X-ray computed tomography, a non destructive method never used previously to investigate fatigue damage in composite materials. Two different levels of load were considered: a low load corresponding to 30% of the tensile failure load and a higher load equal to 50% of tensile failure. The number of cycles of 10000 was kept constant for both loading conditions. Damage inspection revealed the presence of transverse ply cracks, which increase in number with the increasing load; splits that propagate along the loading direction with load, delamination at the ply interfaces, and a few isolated fibre breaks along the splits. A micromechanistic characterisation of damage was conducted, illustrating the interactions between damage and microstructure for the various types of damage detected. Damage growing in the resin rich region and fibre resin rich region resulted in a different form, dependent on the microstructure. An interesting aspect observed was the interacting of damage with toughening particles present in the resin.

Crack shear displacements were assessed measuring by the displacement of fibre broken along the splits. Results showed the dependence of crack shear displacement on the position along the split, decreasing towards to the crack tip.

Finally a qualitative comparison between fatigue and quasi-static loading, performed at the same level of load, was done. The evaluation showed similar behaviour in terms of crack locations and crack shapes. However, delamination was not observed for quasi-static loading. In addition, the same level of load determines higher damage propagation under cyclic loading.

Future Work

Subsequent studies will focus on the quantification of all the damage detected in the preliminary work described in this report, applying the procedures described and used to evaluate the crack opening displacement for splits, also to calculate crack opening displacements for transverse ply cracks. An important aspect will be to compare quantitatively damage caused by quasi-static and fatigue loading, in terms of crack opening displacement for splits and transverse ply cracks, and in terms of the crack opening contours and shape of splits. In addition, damage quantification will use Digital Volume Correlation (DVC). DVC is based on tracking the displacements of small regions of image content, identified in a reference image, in subsequent images generated at increased numbers of cycles or load. Consequently, DVC requires the presence of patterns inside the material to obtain reliable results. The material used in the preliminary experiments did not have any usable microstructural features. However, the specimens to be used for future experiments may contain marker particles, for instance aluminium particles, with the aim to facilitate the identification of material patterns.

Future work will be conducted with the aim to assess the fatigue damage initiation and propagation with the number of the cycles and for different levels of load. The evaluation of the micromechanisms of initiation requires high resolution computed tomography and a consistent number of scans at low cycles, assessing also the influence of load on the nucleation of damage. The estimation of the effect of parameters, such as stacking sequence and ply thickness on the initiation and propagation of damage under fatigue loading is interesting and may represent one of a key issue for investigation. An additional parameter to be investigated, which is likely to affect damage development is the matrix system.

An improved resolution will allow the number of fibre breaks to be monitored and the presence of clusters of fibres breaks to be correlated with the number of cycles for different load levels.

The next step consists of evaluating how damage mechanisms interact with each other; thereby seeking to understand which phenomena lead to failure and how damage propagation is related to the material properties and microstructure. The overall purpose is to find a link between damage growth and failure that allows the

development of a model for fatigue in composites. Performing *in situ* tests to defined numbers of cycles and loads will allow the statistical variability of composite microstructure and behaviour to be quantified. Considering different specimens tested at different numbers of cycles, it is not possible to link directly the current level of damage with the previous number of cycles because damage accumulation is unknown. *In situ* experiments require the design of a load rig to transfer cycling loadings to the specimens.

As discussed previously, different parameters may be taken into account, such as different matrix materials, geometry or stacking layup, to evaluate differences in terms of damage mechanisms and failure.

Computational models represent a challenge to predict damage propagation for composites under fatigue loading. An assessment of numerical models in the literature will be carried out in order to understand their limitations and their potential for application. Based on experimental observations, suitable computational models will be calibrated and validated, so as to describe mechanisms of damage evolution and to develop the capability to perform virtual testing.

Gantt Chart

ID	Task Name	Start	Finish	Duration
1	Proposal for synchrotron SLS	03/09/2012	14/09/2012	2w
2	9 Month Viva	03/09/2012	28/09/2012	4w
3	Crack Opening Displacement for transverse ply cracks	01/10/2012	05/10/2012	1w
4	Comparison between quasi-static and fatigue loading damage quantification	08/10/2012	19/10/2012	2w
5	Working on a proposal paper	22/10/2012	16/11/2012	4w
6	Planning the in situ SRCT experiments	19/11/2012	30/11/2012	2w
7	Design the in situ loading rig	03/12/2012	04/01/2013	5w
8	Prepare specimens	07/01/2013	22/02/2013	7w
9	Swiss Light Source experiments	01/03/2013	15/03/2013	2.2w
10	Analyses SLS data	18/03/2013	31/05/2013	11w
11	Writing Transfer Report	13/05/2013	05/07/2013	8w

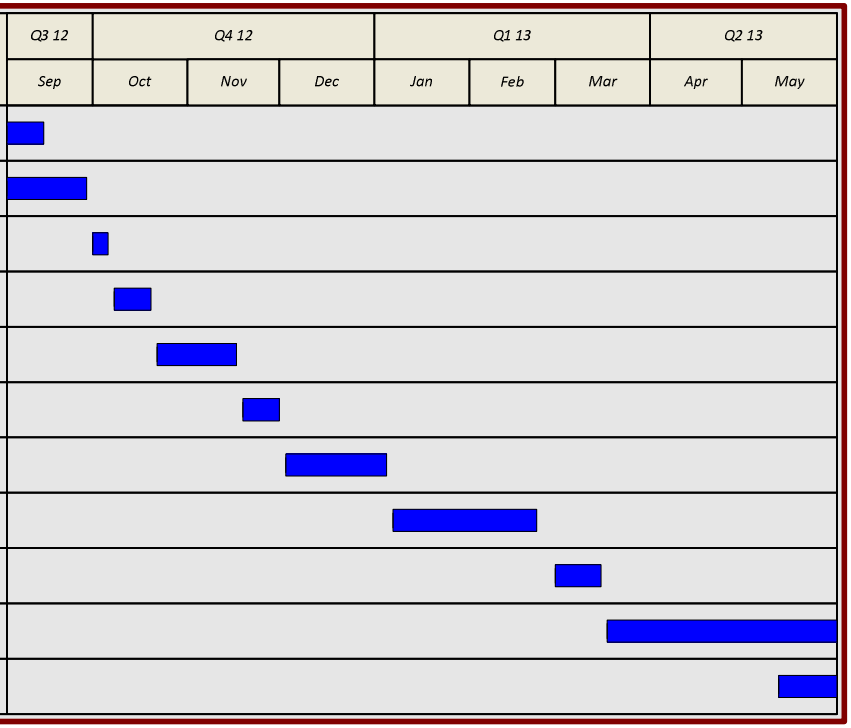

Bibliography

[1] "http://www.hexcel.com/Resources/DataSheets/Prepreg-Data-Sheets/M21_global.pdf," Hexcel.

[2] A. Davies and P. Curtis, "Fatigue in aerospace applications," in *Fatigue in Composites*, CRC Press, 2003, pp. 686-708.

[3] S. Suresh, Fatigue of Materials, Cambridge University Press, 2001 Second Edition.

[4] R. Harrison and M. Bader, "Damage development in CFRP lainates under monotonic and cyclic loading," *Fibre Science and Technology,* vol. 18, pp. 163-180, 1983.

[5] E. Gamstedt and B. Sjogren, "Micromechanisms in tension-compression fatigue of composite laminates containing transverse plies," *Composites Science and Thechnology,* vol. 59, pp. 167-178, 1999.

[6] T. Yokozeki, T. Aoki and T. Ishikawa, "Fatigue growth of matrix in the transverse direction of CFRP laminates," *Composites Science and Technology,* vol. 62, pp. 1223-1229, 2002.

[7] J. Nairn, "Matrix Microcracking in Composites," in *Polymer Matrix Composites*, Pergamon, 1 edition, 2001.

[8] T. Vaughan and C. McCarthy, "Micromechanical modelling of the transverse damage behaviour in fibre reinforced composites," *Composites Sciences and Technology,* vol. 71, pp. 388-396, 2011.

[9] C. Galiotis and C. Koimtzoglou, "The effect of the interface on the fatigue performance of fibre composites," in *Fatigue in composites, Harris*, CRC Press, 2003, pp. 147-172.

[10] L. Drzal and M. Madhukar, "Fibre-matrix adhesion and its relationship to composite mechanical properties," *Journal of Materials Science,* no. 28, pp. 569-610, 1993.

[11] K. Garret and J. Bailey, "Multiple transverse fracture in 90° cross-ply laminates of a glass fibre-reinforced polyester," *Journal of Materials Science,* vol. 12, pp. 157-178, 1977.

[12] D. Flaggs and M. Kural, "Experimental determination of the in situ transverse lamina strength in graphyte/epoxy laminates," *Journal of Composites Material,* vol. 16, pp. 103-115, 1982.

[13] S. Hu, J. Bark and J. Nairn, "On the phenomenon of curved microcracks in [(S)/90n]s laminates: their shapes, initiation angle and locations," *Composite Science and Technology,* vol. 47, pp. 321-329, 1993.

[14] J. Nairn, S. Hu and J. Bark, "A critical evaluation of theories for predicting microcracking in composite laminates," *Journal of Materials Science,* vol. 28, pp. 5099-5111, 1993.

[15] T. Hobbiebrunken, M. Hojo, T. Adachi, C. D. Jong and B. Fiedler, "Evaluation of interfacial strength in CF/epoxies using FEM and in-situ experiments," *Composites, Part A: applied science and manufacturing,* vol. 37, pp. 2248-2256, 2006.

[16] D. Allen, C. Harris, S. Groves and R. Norvell, "Characterization of stiffness loss in cross-ply laminates with curved matrix cracks," *Journal of Composites Material,* vol. 22, pp. 71-80, 1988.

[17] M. Lafaire-Frenot and C. Henaff-Gardin, "Formation of growth of 90 ply fatigue cracks in carbon/epoxy lamiantes," *Composites Sciece and Technology,* vol. 40, pp. 307-324, 1991.

[18] H. Mar and J. Daken, "Splitting initiation and propagation in notched unidirectional graphite/epoxy composites under tension-tension cyclic loading," *Composite Structures,* vol. 4, pp. 111-133, 1985.

[19] A. Garg, "0 splits initiation in fiber reinforced composites," *Engineering Fracture Mechanics,* vol. 24, pp. 255-261, 1986.

[20] S. Spearing and P. Beaumont, "Fatigue damage mechanics of composite materials. I: Experimental measurement of damage and post-fatigue properties," *Composite Sciences and Technology,* vol. 44, pp. 159-168, 1992.

[21] A. Moffat, P. Wright, J.-Y. Buffiere, I. Sinclair and S. Spearing, "Micromechanics of damage in 0° splits in a [90/0]s composite material using synchrotron radiation computed tomography," *Scripta Materialia,* vol. 59, pp. 1043-1046, 2008.

[22] T. Johannesson, P. Sjoblom and R. Selden, "The detailed structure of delamination fracture surfaces in graphite/epoxy laminates," *Journal of Materials Science,* vol. 19, pp. 1171-1177, 1984.

[23] R. Pipes and N. Pagano, "Interlaminar stresses in composite laminates under uniform axial extension," *Journal of Composite Materials,* vol. 4, pp. 538-548, 1970.

[24] E. S. Greenhalgh, C. Rogers and P. Robinson, "Fractographic observations on delamination growth and the subsequent migration through the laminate," *Composite Science and Technology,* vol. 69, pp. 2345-2351, 2009.

[25] J. Reeder, "An evaluation of mixed-mode delamination failure criteria," Hampton, Virginia, 1992.

[26] E. S. Greenhalgh, "Delamination growth in carbon-fibre composite structures," *Composite Structures,* vol. 23, pp. 165-175, 1993.

[27] M. Gilchrist and N. Svensson, "A fractographic analysis of the delamination within multidirectional carbon/epoxy laminates," *Composite Science and Technology,* vol. 55, pp. 195-207, 1995.

[28] A. Scott, M. Mavrogordato, P. Wright, I. Sinclair and S. Spearing, "In situ fibre fracture measurement in carbon-epoxy laminates using high resolution computed tomography," *Composites Science and Technology,* vol. 71, pp. 1471-1477, 2011.

[29] C. Marston, B. Gabbitas, J. Adams, S. Nutt, P. Marshall and C. Galiotis, "Failure characteristics in carbon/epoxy composites tows," *Composites Part A,* vol. 27 A, pp. 1183-1194, 1996.

[30] P. Wright, X. Fu, I. Sinclair and S. Spearing, "Ultra high resolution computed tomography of damage in notched carbon fiber-epoxy composites," *Journal of Composite Materials,* vol. 42, pp. 1993-2002, 2008.

[31] K. Pickering, M. Bader and A. Kimber, "Damage accumulation during the failure of uniaxial carbon fibre composites," *Composites Part A,* vol. 29 A, pp. 435-441, 1998.

[32] B. Rosen, *AIAA J.,* vol. 2, 1964.

[33] S. Phoenix and I. Beyerlein, "Statistical Strength Theory for Fibrous Composite Materials," in *Comprehensive Composite Materials*, Elsevier Science, 2000, pp. 559-639.

[34] C. Marston, B. Gabbitas, J. Adams, P. Marshall and C. Galiotis, "Measuremnt of stress concentration around fibre breaks in carbon-fibre/epoxy-resin composite tows," *Composites Sciences and Technology,* vol. 57, pp. 913-923, 1997.

[35] J. M. Hedgepeth, "Stress concentration in filamentary structures," Washington, 1961.

[36] M. Miner, "cumulative damage in fatigue," *Journal of Applied Mechanics,* vol. 12, pp. 159-164, 1945.

[37] M. Owen and R. Howe, "The accumulation of damage in a glass-reinforced plastics under tensile and fatigue loading," *Journal of Physics D: Applied Physics,* vol. 5, pp. 1637-1649, 1972.

[38] Z. Hashin and A. Rotem, "A cumulative danage theory of fatigue failure," *Materials Science and Engineering,* vol. 34, pp. 147-160, 1978.

[39] N. Post, S. Case and J. Lesko, "Modelling the variable amplitude fatigue of composite materials: A review and evaluation of the state of the art for spectrum loading," *International Journal of Fatigue,* vol. 30, pp. 2064-2086, 2008.

[40] J. Schaff and B. Davidson, "Life prediction methodology for composite structures. Part 1-constant amplitude and two stress level fatigue," *Journal of Composite Materials,* vol. 31, pp. 128-157, 1997.

[41] J. Schaff and B. Davidson, "Life prediction methodology for composite structures. Part II-spectrum fatigue," *Journal of Composite Materials,* vol. 31, pp. 158-181, 1997.

[42] T. Adams, R. Dickson, C. Jones, H. Reiter and B. Harris, "A power law fatigue damage model for fibre-reinforced plastic laminates," *Journal of Mechanical Engineering Science,* vol. 200, pp. 155-166, 1986.

[43] K. Reifsnider and R. Jamison, "Fracture of fatigue-loaded composite laminates," *International Journal of Fatigue,* 1982.

[44] S. Spearing and P. Beaumont, "Fatigue damage mechanics of composite materials Part III: Prediction of post-fatigue strength," *Composite Science and Technology,* vol. 44, pp. 299-307, 1992.

[45] H. Hahn and R. Kim, "Proof testing of composite materials," *Journal of Composite Materials,* vol. 9, pp. 297-311, 1975.

[46] P. Chou and R. Croman, "Residual strength in fatigue based on the strength-life equal rank assumption," *Journal of Composite Materials,* vol. 12, pp. 177-194, 1978.

[47] B. Harris, Engineering Composite Materials, Secon Edition, London: IOM Communications, 1999.

[48] P. Beaumont and B. Harris, "Carbon Fibres: Their Composites and applications," in *Prooceding of an International Conference on Carbon Fibres: Their Composites and applications*, London, 1972.

[49] S. Spearing and P. Beaumont, "Fatigue damage mechanics of composite materials Part IV: Prediction of post-fatigue stiffness," *Composites Science and Technology,* vol. 44, pp. 309-317, 1992.

[50] S. Subramanian, K. Reifsnider and W. Stinchcomb, "A cumulative damage model to predict the fatigue life of composite laminates including the effect of a fibre-matrix interphase," *International Journal of Fatigue,* vol. 17, pp. 343-351, 1995.

[51] T. O'Brein, M. Rigamonti and C. Zanotti, "Tension fatigue analysis and life prediction for composite laminates," *International Journal of fatigue,* vol. 11, pp. 379-393, 1989.

[52] D. Song and N. Otani, "Fatigue life prediction of cross-ply composite laminates," *Materials Science and Engineering ,* vol. A238, pp. 329-335, 1997.

[53] Y. Dzenis, "Cycle-based analysis of damage and fatigue in advanced composites under fatigue. 1. Experimental observation of damage development within loading cycles," *International Journal of Fatigue,* vol. 25, pp. 499-510, 2003.

[54] Y. Dzenis, "Cycle-based analysis of damage and fatigue in advanced composites under fatigue. 2. Stochastic mesomechanics modelling," *International Journal of Fatigue,* vol. 25, pp. 511-520, 2003.

[55] N. Lauws and M. H. G.J. Dvorak, "Stiffness changes in unidirectional composites cause by crack systems," *Machanics of Materials,* vol. 2, pp. 123-137, 1983.

[56] R. Talreja, "Transverse cracking and stiffness reduction in composite laminates," *Journal of Composite Materials,* vol. 19, pp. 355-375, 1985.

[57] R. Talreja, "Stiffness properties of composite laminates with matrix cracking and interior delamination," *Engineering Fracture Mechanics,* vol. 25, pp. 751-762, 1986.

[58] D. Allen, C. Harris and S. Groves, "A thermomechanical constitutive theory for elastic composites with distributed damage - I: theoretical development," *International Journal Solid Structures,* vol. 23, pp. 1301-1318, 1987.

[59] D. Allen, C. Harris and S. Groves, "A thermomechanical constitutive theory for elastic composites with distributed damage - II: Application to matrix cracking in laminated composites," *International Journal Solid Structures,* vol. 23, pp. 1319-1338, 1987.

[60] C. Sun and R. Vaidya, "Prediction of composite properties from a representative volume element," *Composites Science and Technology,* vol. 56, pp. 171-179, 1996.

[61] M. Shokrieh and L. Lessard, "Progress fatigue damage modelling of composite materials, Part I: Modeling," *Journal of Composite Materials,* vol. 34, pp. 1056-1080, 2000.

[62] E. N. Landis and D. Keane, "X-ray microtomography," *Material Characterization,* vol. 61, pp. 1305-1316, 2010.

[63] T. M. Buzug, Computed Tomography, Springer, 2008, pp. 1-59.

[64] T. Lauberberger and J. Luberberger, *Technik der medizinischen Radiologie. Diagnostik, Strahlenterapie, Strahlenschutz,* Cologne, 1999.

[65] J. Hsieh, Computed Tomography: Principles, Design, Artifacts, and Recent Advances, Second ed., SPIE Press and Wiley-Interscience, 2009.

[66] ImPACT, 2005, Available: http://www.impactscan.org/impactcourseslides.htm.

[67] "http://www.matweb.com/search/datasheet.aspx?matguid=50512b22a4b84334b177966a2469f736&ckck=1,".

[68] A. Moffat, "Handover report: In situ calibration of cohesive zone models for composite damage," 2007.

[69] D. Shanmugam, F. Chen, E. Siores and M. Brandt, "Comparative study of jetting machining technologies over laser machining technology for cutting composite materials," *Composite Structures,* vol. 57, pp. 289-296, 2002.

[70] *Standard Test Method for Tension-Tension Fatigue of Pplymer Matrix Composite Materials,* West Conshohocken, United States: ASTM International, 2002.

[71] P. Wright, A. Moffat, I. Sinclair and S. Spearing, "High resolution tomographic imaging and modelling of notch tip daamge in laminate composites," *Composites Science and Technology,* vol. 70, pp. 1444-1452, 2010.

[72] "Instron," Available: http://www.instron.co.uk/wa/product/ElectroPuls-E1000-All-Electric-Instrument.aspx?ref=http://www.google.co.uk/url.

[73] "Instron", Available: www.instron.pl/wa/library/StreamFile.aspx?doc=2341.

[74] "μ-VIS: Multidisciplinary, Multiscale, Microtomographic Volume Imaging," μ-VIS Centre, University of Southampton, Available: http://www.southampton.ac.uk/muvis/.

[75] "Nikon", Available: http://www.nikonmetrology.com/en_EU/Products/X-ray-and-CT-Inspection/Computed-Tomography/XT-H-225-Industrial-CT-Scanning/(brochure).

[76] "Paul Scherrer Institut", Available: http://www.psi.ch/.

Appendix

Test	R	ν (Hz)	N (cycles)	Max Load (N)
e_1.1	0,10	10	10000	108
e_2.1	0,10	10	100	324
e_2.2	0,10	10	1000	324
e_2.3	0,10	10	10000	324
e_3.1	0,10	10	100	540
e_3.2	0,10	10	1000	540
e_3.3	0,10	10	10000	540
e_4.1	0,10	10	100	648
e_4.2	0,10	10	1000	648

Table A. 1 - Parameters of preliminary fatigue tests

Test	R	ν (Hz)	N (cycles)	Max Load (N)
Low load	0.10	10	10000	300 (30% σ_f)
High Load	0,10	10	10000	450 (50% σ_f)

Table A. 2 - Parameters of fatigue tests

Specimen	Scan Condition
Pre-fatigue Low Load	unloaded (38 N) loaded (269 N)
Pre-fatigue High Load	unloaded (50 N) loaded (450 N)
Pre-fatigue High Load, Tips	unloaded (50 N) loaded (450 N)
Quasi-static Low Load	loaded (302 N)
Quasi-static High Load	loaded (454 N)

Table A. 3 – Specimens performed at Swiss Light Source and correspondent scan conditions